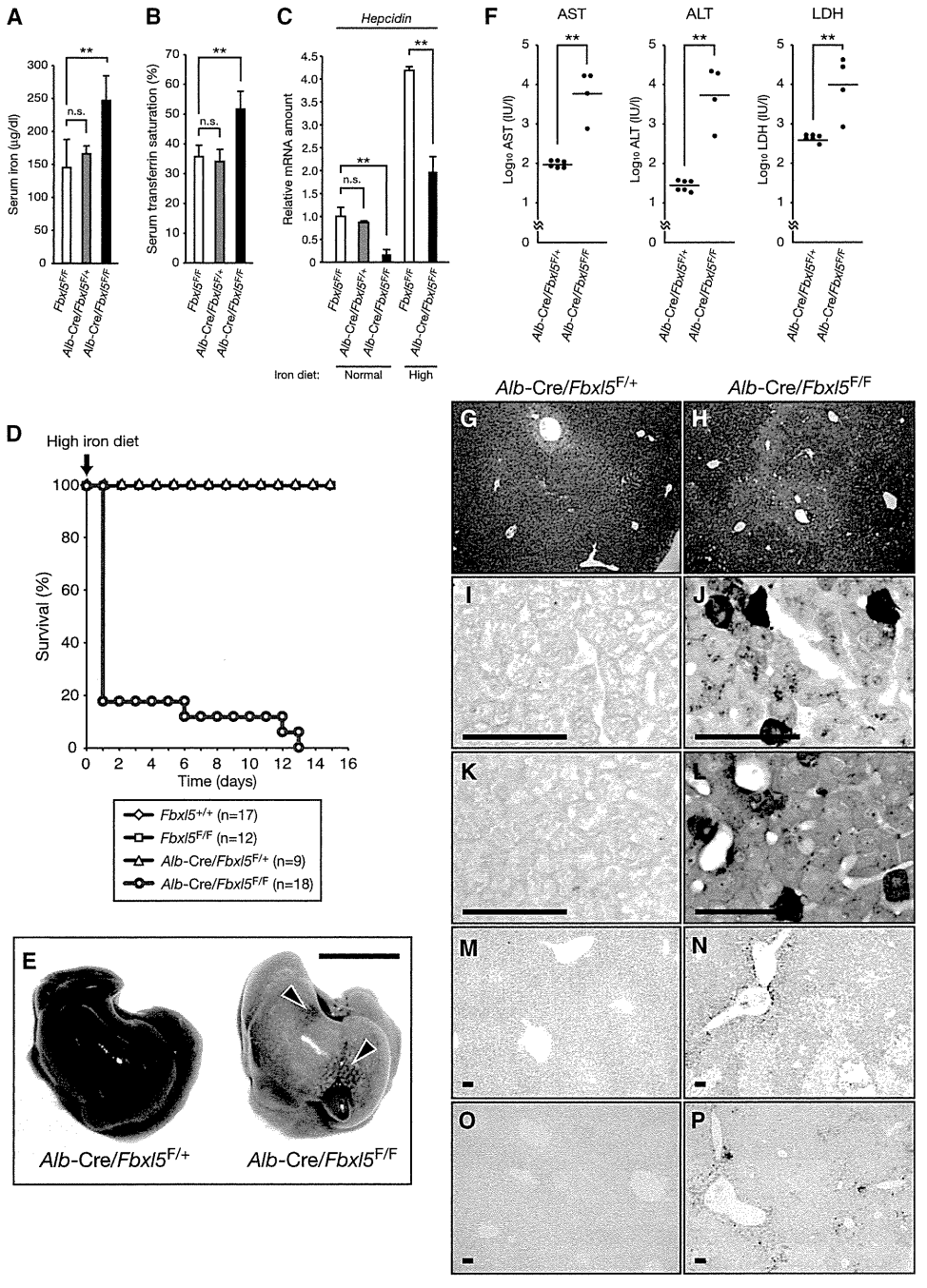

Figure 6. Fatal Liver Failure in *Alb*-Cre/*Fbxl5*$^{F/F}$ Mice Fed a High-Iron Diet

(A) Serum nonheme iron concentration in *Fbxl5*$^{F/F}$ (n = 4), *Alb*-Cre/*Fbxl5*$^{F/+}$ (n = 6), and *Alb*-Cre/*Fbxl5*$^{F/F}$ (n = 7) mice at 16–32 weeks of age. Data are mean ± SD. n.s., not significant. **p < 0.01 (Student's t test).

(B) Serum transferrin saturation in *Fbxl5*$^{F/F}$ (n = 3), *Alb*-Cre/*Fbxl5*$^{F/+}$ (n = 6), and *Alb*-Cre/*Fbxl5*$^{F/F}$ (n = 8) mice at 16–32 weeks of age. Transferrin saturation was calculated from measured total (TIBC) and unsaturated (UIBC) iron-binding capacities. Data are mean ± SD. **p < 0.01 (Student's t test).

(C) RT and real-time PCR analysis of hepcidin mRNA in the liver of 16-week-old mice of the indicated genotypes fed a normal diet or exposed to a high-iron diet for 1 day. Normalized data are expressed relative to the corresponding value for control mice (*Fbxl5*$^{F/F}$ mice fed a normal diet) and are mean ± SEM (n = 3 mice per group). **p < 0.01 (Student's t test).

(D) Kaplan-Meier survival curves for 6-week-old mice of the indicated genotypes after the start of a high-iron diet.

(E) Gross appearance of the liver of 6-week-old *Alb*-Cre/*Fbxl5*$^{F/+}$ and *Alb*-Cre/*Fbxl5*$^{F/F}$ littermates at 1 day after the start of a high-iron diet. Arrowheads indicate bleeding. Scale bar, 10 mm.

(F) Serum AST, ALT, and LDH activities in 6-week-old *Alb*-Cre/*Fbxl5*$^{F/+}$ (n = 6) and *Alb*-Cre/*Fbxl5*$^{F/F}$ (n = 4) mice at 1 day after the start of a high-iron diet. The results are plotted on a logarithmic ordinate, and horizontal lines indicate mean values. **p < 0.01 (Student's t test).

hepcidin in the liver of these mice. They further suggested that liver-specific ablation of FBXL5 results in systemic iron overload as a result of a reduced level of hepcidin secretion from the liver.

Fatal Liver Failure in *Alb*-Cre/*Fbxl5*$^{F/F}$ Mice Fed a High-Iron Diet

Given that hepcidin expression was downregulated in *Alb*-Cre/*Fbxl5*$^{F/F}$ mice, we next examined the effect of iron overload in these animals fed a high-iron diet. Whereas all control mice remained alive, most *Alb*-Cre/*Fbxl5*$^{F/F}$ mice died within 1 day, and the rest ate very little of the diet and lost weight, finally dying of starvation within 2 weeks (Figure 6D). Macroscopic examination of the *Alb*-Cre/*Fbxl5*$^{F/F}$ mice revealed prominent hemorrhage on the surface of the fatty liver (Figure 6E). Both prothrombin time (PT) and activated partial thromboplastin time (APTT) were significantly increased for *Alb*-Cre/*Fbxl5*$^{F/F}$ mice on the high-iron diet compared with those for *Fbxl5*$^{F/F}$ mice (Figure S6D), suggestive of a severe coagulopathy in the former animals. Serum levels of hepatic enzymes such as aspartate aminotransferase (AST), alanine aminotransferase (ALT), and lactate dehydrogenase (LDH) were also increased ~100-fold in these animals (Figure 6F), suggestive of an acute progressive destruction of hepatocytes. Changes in biliary tract enzymes were smaller than those in hepatic enzymes (Table S2). Histological analysis revealed massive cell death, predominantly in the area around portal veins, in the FBXL5-deficient liver (Figures 6G and 6H). DAB-enhanced Perls or Turnbull staining also revealed the accumulation of ferrous iron in the hepatocytes of *Alb*-Cre/*Fbxl5*$^{F/F}$ mice (Figures 6I–6L), whereas detection of 4-HNE-modified proteins revealed a marked increase in oxidative stress (Figures 6M and 6N). TUNEL-positive cells were also observed among hepatocytes of *Alb*-Cre/*Fbxl5*$^{F/F}$ mice (Figures 6O and 6P). Furthermore, oxidative stress and cell death in the liver were markedly attenuated by the addition of NAC to the drinking water of *Alb*-Cre/*Fbxl5*$^{F/F}$ mice fed the high-iron diet (Figure S6E). On the other hand, *Irp2*$^{-/-}$ mice did not die when fed a high-iron diet (n = 6, data not shown), probably because the accumulation of ferrous iron was much less pronounced than was that of ferric iron in these animals (Figure S6F). Given that the high-iron diet had little effect on the iron content of other organs of *Alb*-Cre/*Fbxl5*$^{F/F}$ mice (data not shown), these results indicated that *Alb*-Cre/*Fbxl5*$^{F/F}$ mice fed such a diet died of acute liver failure resulting from iron excess. Collectively, our observations implicate FBXL5 in the regulation of iron homeostasis both at the systemic level and in the liver.

DISCUSSION

We have shown that the loss of FBXL5 results in upregulation of IRP expression and activity, leading to fatal damage in embryos or the adult liver due to the excessive accumulation of ferrous iron. Our genetic evidence suggests that IRP2 is the major target of the SCF^{FBXL5} E3 ligase. Our findings further indicate that FBXL5 plays a central role in the maintenance of appropriate concentrations of intracellular iron and is essential for embryonic development as well as for normal postnatal liver physiology in mice.

Regulation of IRP activity is essential for cells to maintain an appropriate cytosolic LIP, thereby avoiding deleterious iron deficiency and preventing iron excess. FBXL5 recognizes both IRP1 and IRP2 and promotes their degradation in an iron-dependent manner. Our results now indicate that iron-dependent degradation of IRPs mediated by FBXL5 is pivotal for regulation of their activity as well as for iron homeostasis in mice. FBXL5 also senses intracellular iron through direct iron binding to its hemerythrin domain, resulting in FBXL5 stabilization (Salahudeen et al., 2009; Vashisht et al., 2009). Thus, FBXL5 acts as a sensor of the cytosolic LIP that negatively regulates this pool through degradation of IRPs.

Maintenance of the cytosolic LIP at an appropriate level is crucial, especially in cells exposed to iron overload. We found that *Fbxl5*$^{-/-}$ embryos die manifesting iron accumulation in the early placenta, and that *Fbxl5*$^{-/-}$ blastocysts do not survive under iron-replete conditions. These results suggest that FBXL5 is a key regulator that confers resistance to stress resulting from iron overload. During embryogenesis, FBXL5 plays an essential role in the early placental regions. Given that mice lacking the iron-exporting protein ferroportin, which transfers iron from the extraembryonic visceral endoderm (early placenta) into the embryo, die in utero (Donovan et al., 2005), these early placental regions appear to be essential for iron delivery to embryos, and they thereby need to endure stress attributable to iron overload. FBXL5 appears to protect these iron-transferring cells from damage due to excess iron.

FBXL5 also plays an essential role in normal postnatal liver physiology by preventing systemic iron overload. Hereditary hemochromatosis is a genetic disorder that leads to iron overload in the liver and other organs. Complications of this disease include liver cirrhosis, cancer, diabetes, and heart failure. To date, hereditary hemochromatosis has been attributed to defects in five genes, four of which give rise to recessive disorders (De Domenico et al., 2008). All recessive forms of the disease are associated with molecular defects in hepatocytes and are caused by inappropriately low levels of hepcidin expression. We have now shown that liver-specific ablation of FBXL5 results in downregulation of hepcidin expression and consequent systemic iron overload. Therefore, hepatic expression of FBXL5 might also be a determinant of iron overload disorders.

Iron overload status in FBXL5-deficient mice differs substantially from that in other mice showing simple systemic iron overload in terms of the valence of the accumulating iron (Fe^{2+} or Fe^{3+}). FBXL5-deficient mice manifest accumulation of dangerous ferrous iron (Fe^{2+}), whereas many other animal models such as mice deficient in Hfe1 (Zhou et al., 1998), Hfe2 (Niederkofler et al., 2005), or hepcidin (Lesbordes-Brion et al., 2006) exhibit accumulation of ferric iron (Fe^{3+}) in the liver as a result of defective hepcidin production. This point is key to understanding iron metabolism in *Alb*-Cre/*Fbxl5*$^{F/F}$ mice, which

(G–P) Histological analysis of the liver of 6-week-old *Alb*-Cre/*Fbxl5*$^{F/F}$ mice (H, J, L, N, and P) and control *Alb*-Cre/*Fbxl5*$^{F/+}$ littermates (G, I, K, M, and O) at 1 day after the start of a high-iron diet. Hematoxylin and eosin staining is shown in (G) and (H), DAB-enhanced Perls staining is shown in (I) and (J), DAB-enhanced Turnbull staining is shown in (K) and (L), immunohistochemical staining with antibodies to 4-HNE is shown in (M) and (N), and TUNEL staining is shown in (O) and (P). Scale bars, 100 μm. See also Figure S6 and Table S2.

fail to establish two barriers that protect against dietary iron overload: the hepcidin-dependent intestinal barrier against iron hyperabsorption, and the FBXL5-dependent intracellular barrier against an inappropriate increase in the LIP. The aforementioned other mutant mice retain the latter barrier, which minimizes an inappropriate increase in the LIP. Thus, hepatic FBXL5 deficiency gives rise to iron poisoning that is more severe than that that results from simple systemic iron overload due to dietary iron excess.

Hepatic iron overload is a pathophysiologic feature of nonalcoholic steatohepatitis (NASH), chronic liver disease associated with hepatitis C virus infection, and hepatocellular carcinoma (Sorrentino et al., 2009). Excess ferrous iron generates hydroxyl radicals that give rise to chronic inflammation, DNA damage, genetic instability, and tumorigenesis as a result of oxidative stress. Although iron accumulation itself may not initiate chronic liver disease, it has a detrimental effect on disease progression. We have now shown that liver-specific ablation of FBXL5 results in an increased hepatic iron content, systemic iron overload, and acute fatal liver failure in the presence of dietary iron overload. *Alb*-Cre/*Fbxl5*$^{F/F}$ mice develop steatosis and inflammation of the liver, reminiscent of human NASH, likely as a result of mitochondrial damage. Increased serum iron levels might worsen the liver damage in *Alb*-Cre/*Fbxl5*$^{F/F}$ mice. Thus, we speculate that a reduced level of FBXL5 expression in the human liver might give rise to a vicious cycle of liver damage and contribute to the progression of chronic inflammation and liver cancer.

EXPERIMENTAL PROCEDURES

Generation of *Fbxl5*$^{-/-}$ and *Fbxl5*$^{-/-}$*Irp2*$^{-/-}$ Mice

The targeting vector for *Fbxl5* was constructed by replacement of a 3.1 kb fragment of genomic DNA containing exons 4 and 5 of *Fbxl5* with IRES-*lacZ* and PGK-*neo*-poly(A)-loxP cassettes. A diphtheria toxin A (DT-A) cassette was ligated at the 3′ end of the targeting construct. Maintenance, transfection, and selection of mouse ESCs were performed as described previously (Nakayama et al., 1996). Mutant ESCs were microinjected into C57BL/6 blastocysts, and resulting chimeras were mated with C57BL/6 mice. Heterozygous offspring were intercrossed to produce homozygous mutant animals and their littermate controls. For assessment of their growth capability, preimplantation embryos were cultured as described previously (Nishiyama et al., 2009). All mice in this study were backcrossed to the C57BL/6 background for more than six generations. *Fbxl5*$^{+/-}$ mice were also crossed with *Irp2*$^{-/-}$ mice (LaVaute et al., 2001) obtained from Mutant Mouse Regional Resource Centers. *Fbxl5*$^{+/-}$*Irp2*$^{+/-}$ offspring were intercrossed to produce *Fbxl5*$^{-/-}$*Irp2*$^{-/-}$ animals and their littermate controls.

Generation of Conditional Knockout Mice

The 5′ and 3′ regions of homology in the targeting vector for *Fbxl5* consisted of a 1.2 kb fragment of intron 3 and an 8.5 kb fragment spanning introns 3 and 7, respectively. The neomycin-resistance gene (*neo*) flanked by loxP sites was isolated from the plasmid pL2-Neo(2) (kindly provided by D.R. Littman) (Gu et al., 1993) and inserted upstream of exon 4 of *Fbxl5*. A loxP site was also inserted downstream of exon 5. ES clones that had undergone homologous recombination were transfected with pMC-Cre (kindly provided by D.R. Littman) to excise the loxP-*neo* cassette. Mutant ESCs were then microinjected into C57BL/6 blastocysts, and the resulting chimeras were mated with C57BL/6 mice. Heterozygous offspring were intercrossed to produce homozygous mutant animals (*Fbxl5*$^{F/F}$). *Fbxl5*$^{F/F}$ mice were then crossed with *Alb*-Cre transgenic mice (Postic and Magnuson, 2000) obtained from The Jackson Laboratory to produce *Alb*-Cre/*Fbxl5*$^{F/F}$ mice. A high-iron diet was formulated by supplementation of CA-1 (containing 0.03% [w/w] ferric citrate; CLEA Japan) with 2% (w/w) ferric citrate. All animals were maintained under the specific pathogen-free (SPF) condition, and all experiments were approved by the animal ethics committee of Kyushu University.

Iron Histochemistry

Mice (pregnant for analysis of embryos) were anesthetized by intravenous injection of pentobarbital sodium (648 mg/kg) and were then perfused consecutively with 50 mM hydrogen sulfide in deionized water and with 4% paraformaldehyde in phosphate-buffered saline. Iron was detected in cryostat sections by enhanced Perls or Turnbull staining. Tissue sections were washed with deionized water, incubated for 30 min with Perls reagent (5% potassium ferrocyanide, 5% HCl) or with Turnbull reagent (5% potassium ferricyanide, 5% HCl), and then washed again in deionized water before incubation first for 15 min with unactivated DAB (0.05% DAB in deionized water) and then for 10 min with activated DAB (0.05% DAB, 1% H_2O_2). Tissue sections of control and mutant mice were stained at the same time to allow monitoring and detection of nonspecific staining.

Whole-Mount In Situ Hybridization

Whole-mount in situ hybridization was performed as described previously (Nishiyama et al., 2009). An FBXL5 antisense riboprobe corresponding to nucleotides 396–765 of the cDNA was synthesized with the use of a DIG RNA labeling kit (Roche).

RT and Real-Time PCR Analysis

RT and real-time PCR analysis was performed as described previously (Onoyama et al., 2011). Purification of mRNA from embryos was performed with the use of a TurboCapture mRNA Kit (QIAGEN). The sequences of the PCR primers (forward and reverse, respectively) were: 5′-GGTGATCCATACA CACCTGGCTT-3′ and 5′-TGATGACTGAGATGGCGGAA-3′ for TfR1; 5′-CC TATCTCCATCAACAGAT-3′ and 5′-TGCAACAGATACCACACTG-3′ for hepcidin 1 (Hamp1); and 5′-GGACCCGAGAAGACCTCCTT-3′ and 5′-GCACATCAC TCAGAATTTCAATGG-3′ for ARBP (attachment region-binding protein). Reactions for ARBP mRNA were performed concurrently on the same plate as those for the test mRNAs, and results were normalized by the corresponding amount of ARBP mRNA.

Immunoblot Analysis

Immunoblot analysis was performed as previously described (Onoyama et al., 2011) with antibodies to IRP1 (sc-14216; Santa Cruz Biotechnology), to p150^{Glued} (610473; BD Transduction Laboratories), to phosphorylated Smad1(Ser$^{463/465}$)/Smad5(Ser$^{463/465}$)/Smad8(Ser$^{426/428}$) (9511; Cell Signaling Technology), to ferritin (F6136; Sigma-Aldrich), to TfR1 (13-6800; Invitrogen), to Hsp90 (610419; BD Biosciences), and to IRP2 (generated by K. Iwai, Osaka University).

Statistical Analysis

Quantitative data are presented as mean ± SEM or ± SD as indicated and were compared between groups with the two-tailed Student's t test as performed with Microsoft Excel software. A p value of <0.05 was considered statistically significant.

SUPPLEMENTAL INFORMATION

Supplemental Information includes Supplemental Experimental Procedures, Supplemental References, six figures, and two tables and can be found with this article online at doi:10.1016/j.cmet.2011.07.011.

ACKNOWLEDGMENTS

We thank T. Rouault for *Irp2*$^{-/-}$ mice; D.R. Littman for pL2-Neo(2) and pMC-Cre; T. Kitamura for pMX-puro; M. Tanaka, Y. Yamada, K. Takeda, M. Sasaki, R. Ugawa, M. Oda, E. Koba, and N. Kinoshita for technical assistance; and D. Kang, S. Toyokuni, S. Sakata, and T. Asano for discussion.

Received: March 30, 2011
Revised: June 23, 2011
Accepted: July 19, 2011
Published: September 6, 2011

REFERENCES

Andrews, N.C., and Schmidt, P.J. (2007). Iron homeostasis. Annu. Rev. Physiol. *69*, 69–85.

Burt, A.D. (2001). Steatosis and steatohepatitis. Curr. Diagn. Pathol. *7*, 141–147.

Cooperman, S.S., Meyron-Holtz, E.G., Olivierre-Wilson, H., Ghosh, M.C., McConnell, J.P., and Rouault, T.A. (2005). Microcytic anemia, erythropoietic protoporphyria, and neurodegeneration in mice with targeted deletion of iron-regulatory protein 2. Blood *106*, 1084–1091.

Cross, J.C., Werb, Z., and Fisher, S.J. (1994). Implantation and the placenta: key pieces of the development puzzle. Science *266*, 1508–1518.

De Domenico, I., McVey Ward, D., and Kaplan, J. (2008). Regulation of iron acquisition and storage: consequences for iron-linked disorders. Nat. Rev. Mol. Cell Biol. *9*, 72–81.

De Domenico, I., Vaughn, M.B., Li, L., Bagley, D., Musci, G., Ward, D.M., and Kaplan, J. (2006). Ferroportin-mediated mobilization of ferritin iron precedes ferritin degradation by the proteasome. EMBO J. *25*, 5396–5404.

Donovan, A., Lima, C.A., Pinkus, J.L., Pinkus, G.S., Zon, L.I., Robine, S., and Andrews, N.C. (2005). The iron exporter ferroportin/Slc40a1 is essential for iron homeostasis. Cell Metab. *1*, 191–200.

Galy, B., Ferring, D., Minana, B., Bell, O., Janser, H.G., Muckenthaler, M., Schümann, K., and Hentze, M.W. (2005). Altered body iron distribution and microcytosis in mice deficient in iron regulatory protein 2 (IRP2). Blood *106*, 2580–2589.

Gu, H., Zou, Y.R., and Rajewsky, K. (1993). Independent control of immunoglobulin switch recombination at individual switch regions evidenced through Cre-loxP-mediated gene targeting. Cell *73*, 1155–1164.

Hentze, M.W., Muckenthaler, M.U., Galy, B., and Camaschella, C. (2010). Two to tango: regulation of Mammalian iron metabolism. Cell *142*, 24–38.

Jin, J., Cardozo, T., Lovering, R.C., Elledge, S.J., Pagano, M., and Harper, J.W. (2004). Systematic analysis and nomenclature of mammalian F-box proteins. Genes Dev. *18*, 2573–2580.

Kautz, L., Meynard, D., Monnier, A., Darnaud, V., Bouvet, R., Wang, R.H., Deng, C., Vaulont, S., Mosser, J., Coppin, H., and Roth, M.P. (2008). Iron regulates phosphorylation of Smad1/5/8 and gene expression of Bmp6, Smad7, Id1, and Atoh8 in the mouse liver. Blood *112*, 1503–1509.

LaVaute, T., Smith, S., Cooperman, S., Iwai, K., Land, W., Meyron-Holtz, E., Drake, S.K., Miller, G., Abu-Asab, M., Tsokos, M., et al. (2001). Targeted deletion of the gene encoding iron regulatory protein-2 causes misregulation of iron metabolism and neurodegenerative disease in mice. Nat. Genet. *27*, 209–214.

Lesbordes-Brion, J.C., Viatte, L., Bennoun, M., Lou, D.Q., Ramey, G., Houbron, C., Hamard, G., Kahn, A., and Vaulont, S. (2006). Targeted disruption of the hepcidin 1 gene results in severe hemochromatosis. Blood *108*, 1402–1405.

MacKenzie, E.L., Iwasaki, K., and Tsuji, Y. (2008). Intracellular iron transport and storage: from molecular mechanisms to health implications. Antioxid. Redox Signal. *10*, 997–1030.

Meguro, R., Asano, Y., Iwatsuki, H., and Shoumura, K. (2003). Perfusion-Perls and -Turnbull methods supplemented by DAB intensification for nonheme iron histochemistry: demonstration of the superior sensitivity of the methods in the liver, spleen, and stomach of the rat. Histochem. Cell Biol. *120*, 73–82.

Meyron-Holtz, E.G., Ghosh, M.C., and Rouault, T.A. (2004a). Mammalian tissue oxygen levels modulate iron-regulatory protein activities in vivo. Science *306*, 2087–2090.

Meyron-Holtz, E.G., Ghosh, M.C., Iwai, K., LaVaute, T., Brazzolotto, X., Berger, U.V., Land, W., Ollivierre-Wilson, H., Grinberg, A., Love, P., and Rouault, T.A. (2004b). Genetic ablations of iron regulatory proteins 1 and 2 reveal why iron regulatory protein 2 dominates iron homeostasis. EMBO J. *23*, 386–395.

Muckenthaler, M.U., Galy, B., and Hentze, M.W. (2008). Systemic iron homeostasis and the iron-responsive element/iron-regulatory protein (IRE/IRP) regulatory network. Annu. Rev. Nutr. *28*, 197–213.

Nakayama, K., Ishida, N., Shirane, M., Inomata, A., Inoue, T., Shishido, N., Horii, I., Loh, D.Y., and Nakayama, K.I. (1996). Mice lacking p27(^{Kip1}) display increased body size, multiple organ hyperplasia, retinal dysplasia, and pituitary tumors. Cell *85*, 707–720.

Nakayama, K.I., and Nakayama, K. (2006). Ubiquitin ligases: cell-cycle control and cancer. Nat. Rev. Cancer *6*, 369–381.

Nemeth, E., Tuttle, M.S., Powelson, J., Vaughn, M.B., Donovan, A., Ward, D.M., Ganz, T., and Kaplan, J. (2004). Hepcidin regulates cellular iron efflux by binding to ferroportin and inducing its internalization. Science *306*, 2090–2093.

Niederkofler, V., Salie, R., and Arber, S. (2005). Hemojuvelin is essential for dietary iron sensing, and its mutation leads to severe iron overload. J. Clin. Invest. *115*, 2180–2186.

Nishiyama, M., Oshikawa, K., Tsukada, Y., Nakagawa, T., Iemura, S., Natsume, T., Fan, Y., Kikuchi, A., Skoultchi, A.I., and Nakayama, K.I. (2009). CHD8 suppresses p53-mediated apoptosis through histone H1 recruitment during early embryogenesis. Nat. Cell Biol. *11*, 172–182.

Onoyama, I., Suzuki, A., Matsumoto, A., Tomita, K., Katagiri, H., Oike, Y., Nakayama, K., and Nakayama, K.I. (2011). Fbxw7 regulates lipid metabolism and cell fate decisions in the mouse liver. J. Clin. Invest. *121*, 342–354.

Postic, C., and Magnuson, M.A. (2000). DNA excision in liver by an albumin-Cre transgene occurs progressively with age. Genesis *26*, 149–150.

Recalcati, S., Alberghini, A., Campanella, A., Gianelli, U., De Camilli, E., Conte, D., and Cairo, G. (2006). Iron regulatory proteins 1 and 2 in human monocytes, macrophages and duodenum: expression and regulation in hereditary hemochromatosis and iron deficiency. Haematologica *91*, 303–310.

Rouault, T.A., and Tong, W.H. (2005). Iron-sulphur cluster biogenesis and mitochondrial iron homeostasis. Nat. Rev. Mol. Cell Biol. *6*, 345–351.

Salahudeen, A.A., Thompson, J.W., Ruiz, J.C., Ma, H.W., Kinch, L.N., Li, Q., Grishin, N.V., and Bruick, R.K. (2009). An E3 ligase possessing an iron-responsive hemerythrin domain is a regulator of iron homeostasis. Science *326*, 722–726.

Sorrentino, P., D'Angelo, S., Ferbo, U., Micheli, P., Bracigliano, A., and Vecchione, R. (2009). Liver iron excess in patients with hepatocellular carcinoma developed on non-alcoholic steato-hepatitis. J. Hepatol. *50*, 351–357.

Vashisht, A.A., Zumbrennen, K.B., Huang, X., Powers, D.N., Durazo, A., Sun, D., Bhaskaran, N., Persson, A., Uhlen, M., Sangfelt, O., et al. (2009). Control of iron homeostasis by an iron-regulated ubiquitin ligase. Science *326*, 718–721.

Wang, J., and Pantopoulos, K. (2011). Regulation of cellular iron metabolism. Biochem. J. *434*, 365–381.

Zhang, N., Liu, J., Ding, X., Aikhionbare, F., Jin, C., and Yao, X. (2007). FBXL5 interacts with p150^{Glued} and regulates its ubiquitination. Biochem. Biophys. Res. Commun. *359*, 34–39.

Zhou, X.Y., Tomatsu, S., Fleming, R.E., Parkkila, S., Waheed, A., Jiang, J., Fei, Y., Brunt, E.M., Ruddy, D.A., Prass, C.E., et al. (1998). HFE gene knockout produces mouse model of hereditary hemochromatosis. Proc. Natl. Acad. Sci. USA *95*, 2492–2497.

KDM7 is a dual demethylase for histone H3 Lys 9 and Lys 27 and functions in brain development

Yu-ichi Tsukada, Tohru Ishitani and Keiichi I. Nakayama

Genes Dev. 2010 24: 432-437
Access the most recent version at doi:10.1101/gad.1864410

RESEARCH COMMUNICATION

KDM7 is a dual demethylase for histone H3 Lys 9 and Lys 27 and functions in brain development

Yu-ichi Tsukada,[1,2,3] Tohru Ishitani,[4] and Keiichi I. Nakayama[1,2,5]

[1]Division of Cell Biology, Medical Institute of Bioregulation, Kyushu University, Higashi-ku, Fukuoka 812-8582, Japan; [2]CREST, Japan Science and Technology Agency (JST), Kawaguchi, Saitama 332-0012, Japan; [3]PRESTO, Japan Science and Technology Agency (JST), Kawaguchi, Saitama 332-0012, Japan; [4]Division of Cell Regulation Systems, Medical Institute of Bioregulation, Kyushu University, Higashi-ku, Fukuoka 812-8582, Japan

Methylation of histone H3 Lys 9 and Lys 27 (H3K9 and H3K27) is associated with transcriptional silencing. Here we show that KDM7, a JmjC domain-containing protein, catalyzes demethylation of both mono- or dimethylated H3K9 and H3K27. Inhibition of KDM7 orthologs in zebrafish resulted in developmental brain defects. KDM7 interacts with the follistatin gene locus, and KDM7 depletion in mammalian neuronal cells suppressed follistatin gene transcription in association with increased levels of dimethylated H3K9 and H3K27. Our findings identify KDM7 as a dual demethylase for H3K9 and H3K27 that functions as an eraser of silencing marks on chromatin during brain development.

Supplemental material is available at http://www.genesdev.org.

Received September 16, 2009; revised version accepted December 31, 2009.

Histone methylation status defines the epigenetic program of a cell by determining chromatin structure and thereby regulating DNA-dependent processes such as transcription (Strahl and Allis 2000; Lachner et al. 2003; Margueron et al. 2005; Martin and Zhang 2005). Histone methylation has also been linked to regulation of neuronal function (Iwase et al. 2007). The recent discovery of histone demethylases revealed that histone methylation is a more dynamic process than previously recognized, and that most identified demethylases show a strict substrate specificity limited to a single methylation site (Bannister et al. 2002; Shi et al. 2004; Klose et al. 2006a; Tsukada et al. 2006; Shi and Whetstine 2007; Cloos et al. 2008; Lan et al. 2008). A number of histone demethylases contain a JmjC domain, and a subfamily of JmjC domain-containing proteins (comprising KIAA1718, PHF8, and PHF2) is evolutionarily conserved from *Caenorhabditis elegans* to humans and is characterized by the presence of a PHD-type zinc finger motif in addition to the JmjC domain (Supplemental Fig. S1A). Whereas the human genes for PHF8 and PHF2 are associated with X-linked mental retardation and hereditary sensory neuropathy type I, respectively (Hasenpusch-Theil et al. 1999; Laumonnier et al. 2005; Abidi et al. 2007; Koivisto et al. 2007), little is known about KIAA1718. Bioinformatic analysis of the JmjC domains of KIAA1718, PHF8, and PHF2 indicated that predicted Fe(II)- and α-ketoglutarate (α-KG)-binding sites are conserved, with the exception of the former in PHF2, and that they share extensive similarity with the JmjC domain of JHDM1/KDM2 (Supplemental Fig. S1B). Conservation of residues within the putative cofactor-binding sites of KIAA1718 suggested that this protein might possess histone demethylase activity, and therefore might also contribute to transcriptional regulation of genes in the nervous system.

[*Keywords*: Demethylase; JmjC; methylation; histone; chromatin; epigenetics]

[5]**Corresponding author.**
E-MAIL nakayak1@bioreg.kyushu-u.ac.jp; FAX 81-92-642-6819.

Article is online at http://www.genesdev.org/cgi/doi/10.1101/gad.1864410.

Results and Discussion

KIAA1718 possesses histone demethylase activity

To examine whether KIAA1718 indeed possesses histone demethylase activity, we generated the mouse protein tagged with the Flag epitope at its C terminus in insect cells (Fig. 1A), and incubated the recombinant protein with histone substrates labeled with ^{3}H at various characterized methyl-lysine or methyl-arginine sites by corresponding histone methyltransferases (HMTs). Histone demethylase activity was monitored by measurement of the release of the labeled demethylation product, formaldehyde. Substantial release of labeled formaldehyde was observed in the reaction mixture containing histone H3 labeled on Lys 9 (H3K9) by G9a, but not in those containing histone substrates modified by other HMTs (Fig. 1B). Consistent with the notion that the observed enzymatic activity was intrinsic to KIAA1718, formaldehyde release from G9a-labeled H3 was dependent on KIAA1718 concentration (Fig. 1C). To ascertain whether the demethylation mediated by KIAA1718 is oxidative in nature, with Fe(II) and α-KG as cofactors, we examined whether the enzymatic activity of KIAA1718 is dependent on these cofactors. The release of formaldehyde mediated by KIAA1718 was indeed found to require both Fe(II) and α-KG (Fig. 1D). Ascorbate was also required for the enzymatic activity, presumably as a result of its ability to regenerate Fe(II) from Fe(III). To verify further that the observed enzymatic activity is attributable to a genuine demethylase, we generated recombinant forms of KIAA1718 that either lack the JmjC or PHD domains or contain a mutation (H282A) in the Fe(II)-binding site in insect cells (Fig. 1E). Analysis of similar amounts of the mutant proteins for histone demethylase activity revealed that deletion of the JmjC domain or mutation of His^{282} abolished the activity of KIAA1718, whereas the PHD domain appeared to be dispensable for such activity (Fig. 1E,F). Together, these results showed that KIAA1718 is a histone demethylase capable of removing methyl groups from H3K9. Given that histone demethylase activity is the first function attributed to KIAA1718, we named this protein KDM7 on the basis of the previously described nomenclature (Allis et al. 2007).

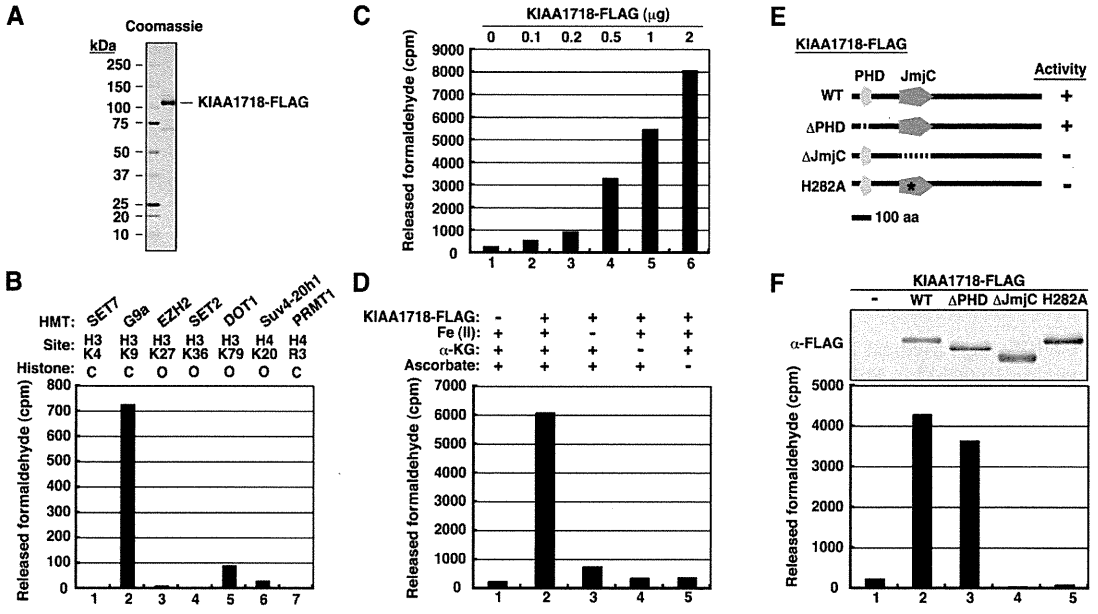

Figure 1. KIAA1718 is a histone demethylase that targets H3K9. (*A*, *right* lane) SDS–polyacrylamide gel electrophoresis with Coomassie blue staining of a C-terminally Flag-tagged recombinant KIAA1718 protein. Molecular size standards are shown in the *left* lane. (*B*) Histone demethylase activity of purified KIAA1718-Flag with various methylated histone substrates. The HMTs used to generate the various substrates and their sites of methylation are indicated. The methylated substrates were generated with the indicated forms of histone ([C] core histone octamer; [O] oligonucleosome) on the basis of the substrate preference of each HMT. The presented counts have been corrected for control counts. (*C*) Histone demethylase activity of the indicated amounts of KIAA1718-Flag. (*D*) Effects of removal of Fe(II), α-KG, or ascorbate from the reaction mixture on the histone demethylase activity of KIAA1718-Flag with G9a-methylated histone substrate. (*E*) Schematic representation of wild-type (WT) and mutant forms of KIAA1718 showing whether they are active (+) or inactive (−) as H3K9 demethylases. (*F*, *bottom* panel) Demethylase activity of purified wild-type or mutant forms of KIAA1718-Flag with G9a-methylated histone substrate. (*Top* panel) The similar amounts of KIAA1718-Flag proteins used in the demethylase assay are revealed by immunoblot analysis with antibodies to Flag (α-Flag).

KDM7 is a dual demethylase for dimethylated and monomethylated H3K9 (H3K9me2/me1) and H3K27me2/me1

To define the substrate and modification state specificity of KDM7, we included core histones as substrates in demethylation reaction mixtures and examined the modification status of individual methylation sites by immunoblot analysis with a series of methylation-specific antibodies. Wild-type KDM7 mediated a marked decrease in the methylation level of both H3K9me2 and H3K27me2, without affecting that of other histone methylation sites (Fig. 2A; Supplemental Fig. S2A). In addition, KDM7 efficiently removed methyl groups from H3K9me2 and H3K27me2 in core histones, but not from those in mono- or oligonucleosomes (Supplemental Fig. S2B,C). These results suggested that KDM7 prefers core histones rather than mono- or oligonucleosomes as substrates, and explain why demethylase activity was not detected by the radioactive formaldehyde release assay with nucleosomal histones methylated by the HMT EZH2 (Fig. 1B). They also suggested that the low level of reactivity apparent in the formaldehyde release assay with oligonucleosomes modified by DOT1 or Suv4-20h1 as substrates does not reflect demethylase activity of KDM7. To refine further the specificity of KDM7, we used methylated peptides as substrates in demethylation reactions and analyzed the removal of methyl groups from the peptides by mass spectrometry. This assay showed that KDM7 removed methyl groups from both H3K9me2 and H3K27me2 (Fig. 2B,C), eliminating the possibility of cross-reaction of antibodies between methylated H3K9 and H3K27 in the immunoblot analysis. KDM7 also demethylated both H3K9me1 and H3K27me1 (Fig. 2B,C), activity that was not apparent by immunoblot analysis (Fig. 2A), probably because demethylation by KDM7 is not highly processive, so that a reduction in the level of monomethylation is masked by production of monomethylated histone from dimethylated histone in a reaction with core histones that contain all three states of methylation, as compared with peptides containing a single monomethylation state. No demethylation was detected with trimethylated H3K9 (H3K9me3) or H3K27me3 peptides. A low level of demethylation activity was also apparent with an H3K36me2 peptide, but no demethylation of H3K36me1 or H3K36me3 was detected (Fig. 2D). The decrease in mass corresponding to a methyl group was not detected in reaction mixtures containing other methylated histone peptides (Supplemental Fig. S3). Together, these data suggested that KDM7 is an authentic histone demethylase with the ability to mediate the direct removal of methyl groups from H3K9me2/me1 and H3K27me2/me1.

Zebrafish KDM7 orthologs possess histone demethylase activity for H3K9/K27 and are expressed predominantly in the brain

To explore the biological function of KDM7 in vivo, we characterized the KDM7 orthologs in zebrafish—LOC321248 and LOC558416, hereafter designated drKDM7a and drKDM7b, respectively (Supplemental Fig. S1A)—both of which were also found to manifest histone demethylase activity toward H3K9me2 and

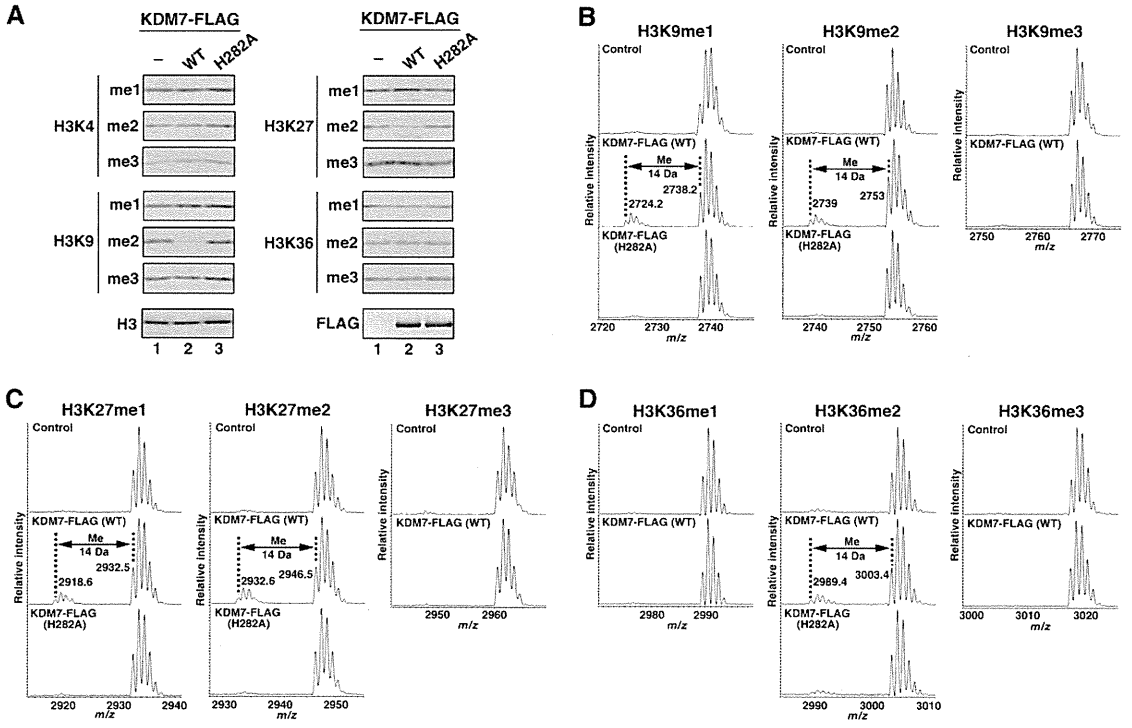

Figure 2. KDM7 is a histone demethylase specific for dimethylated or monomethylated H3K9 or H3K27. (*A*) Calf thymus core histones were incubated in the absence or presence of 5 μg of wild-type or H282A mutant forms of KDM7-Flag, after which histone demethylation was evaluated by immunoblot analysis with antibodies to specific modified histones, as indicated on the *left*. (*B–D*) Mass spectrometric analysis of the demethylase activity of 4 μg of wild-type or H282A mutant forms of KDM7-Flag with methylated H3K9, H3K27, or H3K36 peptide substrates. Numbers represent the masses of the peptide substrates and products.

H3K27me2 in core histones (Supplemental Fig. S4A). We first examined the expression patterns of *kdm7a* and *kdm7b* during development by in situ hybridization. Transcripts corresponding to *kdm7a* and *kdm7b* were detected as early as the post-somitogenesis stage at 24 h post-fertilization (hpf) in the brain and tail bud (Fig. 3A,B), whereas no signals were observed in embryos at 6 or 12 hpf (data not shown). The expression of both *kdm7* genes became prominent in the tectum, hindbrain, fin bud, and gill at 48 hpf (Fig. 3A,B). Corresponding sense probes did not yield any signals at these various stages of development (Supplemental Fig. S4B), indicating that the signals attributed to *kdm7* transcripts were specific.

Zebrafish KDM7 orthologs are required for tectum development

Given that both *kdm7* genes are expressed predominantly in the brain, we examined whether drKDM7 might function in brain development. To examine this possibility, we inhibited the function of drKDM7 with the use of two splicing-blocking antisense morpholino oligonucleotides (MOs) that independently target *kdm7a* or *kdm7b*. We also studied the stable transgenic line Tg(*HuC:Kaede*), which expresses the fluorescent protein Kaede in neurons under the control of the vertebrate neuron-specific promoter of the *HuC* gene, in order to visualize neurons (Sato et al. 2006). The level of mature mRNAs derived from the two *kdm7* genes was reduced specifically in embryos injected with the corresponding MO, but not in those injected with a control MO (Supplemental Fig. S5A). At 48 hpf, embryos that had been subjected to simultaneous injection of both *kdm7* MOs at the one-cell stage manifested a curly tail and marked decrease in size of the tectum (Fig. 3C,D), consistent with the observed expression of *kdm7* in the brain and tail bud. Importantly, the reduction in tectum size was accompanied by the loss of neurons from this region, although neurons in the spinal cord and other regions of the brain were unaffected (Fig. 3D; Supplemental Fig. S5B,C). In contrast, injection of MOs specific for each *kdm7* gene alone elicited only marginal effects compared with those of the control MO, a finding likely attributable to functional redundancy of the two *kdm7* genes. The persistence at 72 hpf of the phenotypes of the embryos injected with both *Kdm7* MOs eliminates the possibility that they were attributable to developmental delay (Fig. 3C; Supplemental Fig. S5B,C). Embryos that had been subjected to simultaneous injection of another set of MOs that independently target *kdm7a* and *kdm7b* also manifested phenotypes (Supplemental Fig. S6) similar to those observed with the original set (Fig. 3C,D), suggesting that the phenotypes were the specific consequence of depletion of *kdm7* transcripts. Coinjection of a validated MO for p53 (Robu et al. 2007) with either of the two independent sets of MOs for *kdm7* did not affect the phenotypes induced by MO-mediated depletion of *kdm7* transcripts (Supplemental Fig. S7), eliminating the possibility that the phenotypes were the result of p53 activation. Given that the phenotypes were not attributable to cell death (Supplemental Fig. S8), drKDM7 might regulate the proliferation or differentiation of neurons. On

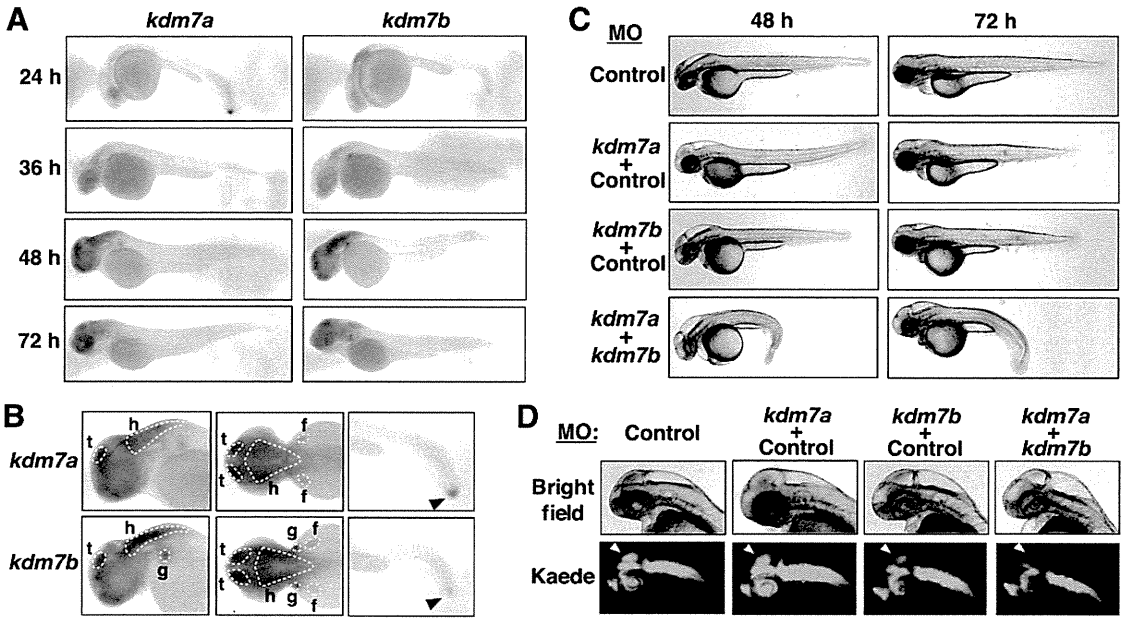

Figure 3. Zebrafish *kdm7* genes are expressed predominantly in brain and are required for tectum development. (*A*) In situ hybridization of whole-mount zebrafish embryos at the indicated stages (hpf) with antisense *kdm7a* or *kdm7b* RNA probes. (*B*) In situ hybridization of whole-mount embryos at 48 hpf (*left* and *middle* panels) or 24 hpf (*right* panels) with antisense *kdm7a* or *kdm7b* RNA probes. Lowercase letters indicate the tectum (t), hindbrain (h), fin bud (f), and gill (g). Arrowheads indicate the tail bud. (*C*) The Tg(*HuC:Kaede*) embryos were injected at the one-cell stage with antisense MOs for *kdm7a* (5 ng) or *kdm7b* (5 ng) or with a control MO (5 or 10 ng for a total of 10 ng of MO) in the indicated combinations. The morphology of the embryos at the indicated times (hpf) was examined by bright-field microscopy. (*D*) Morphology of the head region of embryos at 48 hpf that were injected with MOs as in *C*. (*Bottom* panels) Neurons expressing Kaede under the control of the HuC gene promoter were visualized by fluorescence microscopy. Arrowheads indicate the tectum or presumptive tectal region. Bright-field images are shown in the *top* panels.

the other hand, ectopic overexpression of a fragment of drKDM7a comprising amino acids 1–480 (which manifested demethylase activity similar to that of the full-length protein) achieved by mRNA injection at the one-cell stage resulted in severe developmental defects in zebrafish embryos (Supplemental Fig. S9), suggesting that spatially and temporally regulated expression of drKDM7 is necessary for proper development. Together, these results thus indicated that KDM7 plays an important role in brain development.

KDM7 directly regulates transcription and H3K9me2 and H3K27me2 levels of the follistatin gene

Quantitative RT–PCR analysis revealed that *Kdm7* mRNA was more abundant specifically in the cerebrum and cerebellum than in other mouse tissues, although low levels of *Kdm7* expression were apparent in a wide spectrum of tissues in the mouse (Supplemental Fig. S10A). To investigate the molecular basis for the abnormal brain development in zebrafish embryos depleted of drKDM7, as well as the function of KDM7 in neurons, we examined the effect of KDM7 depletion on the mRNA profile of the mouse neuroblastoma cell line Neuro2A, in which the abundance of KDM7 was found to be greater than that in other cell lines originating from various tissues (Supplemental Fig. S10B). To this end, we stably transfected Neuro2A cells with vectors for two shRNAs—KD1 and KD2—that target two different regions of mouse *Kdm7* mRNA. Quantitative RT–PCR and immunoblot analyses revealed that the amounts of *Kdm7* mRNA and KDM7 protein were markedly decreased in cells transfected with either of these vectors compared with those in parental cells or in cells transfected with a vector for a control shRNA (Fig. 4A,B). Microarray analysis of mRNAs in control cells and in those depleted of KDM7 resulted in the identification of genes whose expression was affected by KDM7 depletion (Supplemental Fig. S10C). One of these genes whose expression was markedly decreased by loss of KDM7 was that for follistatin, on which we initially focused, given that follistatin functions as an endogenous inhibitor of members of the transforming growth factor (TGF)-β superfamily, including activin, which plays an important role in brain development (Hemmati-Brivanlou et al. 1994; Lin et al. 2003; Zhu et al. 2008). We confirmed by quantitative RT–PCR analysis that the abundance of follistatin mRNA was decreased in Neuro2A cells depleted of KDM7 (Fig. 4C). Consistent with the results obtained with Neuro2A cells, depletion of KDM7 by RNAi in primary cultured mouse neurons also resulted in down-regulation of follistatin mRNA (Fig. 4D).

To determine whether the follistatin gene is a direct target of KDM7, we performed a series of chromatin immunoprecipitation (ChIP) experiments to examine its promoter and coding regions in Neuro2A cells (Fig. 4E). This analysis revealed the association of KDM7 with the follistatin gene, predominantly around the transcription start site (Fig. 4F). To investigate the consequences of this association, we analyzed H3K9me2 and H3K27me2 levels in the promoter and coding regions of the gene. Depletion of KDM7 resulted in an increase in both H3K9me2 and H3K27me2 levels around the transcription start site of the gene that appeared to correlate

with KDM7 occupancy (Fig. 4G). Depletion of KDM7 by RNAi in Neuro2A cells did not markedly affect H3K9me3 levels of the follistatin gene (Supplemental Fig. S11A). In contrast, depletion of KDM7 paradoxically increased H3K27me3 levels in the entire region of the gene (Supplemental Fig. S11B), although KDM7 showed no activity toward H3K27me3 in vitro. Given that the regions in which H3K27me3 levels were increased did not correlate with KDM7 occupancy, the observed changes in H3K27me3 levels were most likely an indirect effect of KDM7 depletion. These results suggested that the follistatin gene is a direct target of KDM7-mediated transcriptional activation.

We thus examined whether the zebrafish follistatin gene is dysregulated in *kdm7* morphants with the use of in situ hybridization. Whereas control morphants showed expression of the follistatin gene in an anterior edge region of the tectum at 48 hpf, *kdm7* morphants manifested a substantial decrease in such expression (Fig. 4H). The down-regulation of follistatin gene expression in this particular region was sustained at 60 and 72 hpf (Supplemental Fig. S12A). The corresponding sense probe did not yield any signals at the corresponding stages (Supplemental Fig. S12B). These results thus suggested that KDM7 is recruited to specific regions of the genome, and there functions as an H3K9 and H3K27 demethylase in vivo. To investigate whether follistatin contributes to brain development in zebrafish, we inhibited the function of follistatin with the use of two independent MOs that target the follistatin gene. At 48 hpf, embryos that had been injected with either *follistatin* MO at the one-cell stage manifested a loss of neurons from the tectum region, although neurons in the spinal cord and other regions of the brain were unaffected (Supplemental Fig. S13). Coinjection of the validated MO for p53 did not affect this phenotype (Fig. 4I; Supplemental Fig. S13C). Together, these results indicated that KDM7 contributes to brain development at least in part through regulation of follistatin gene expression.

Methylation of H3K9 and H3K27 is linked to formation of tightly packed chromatin (heterochromatin) and transcriptional silencing (Martin and Zhang 2005). We showed here that KDM7 is a histone demethylase that catalyzes demethylation at both H3K9 and H3K27. Among the JmjC domain-containing histone demethylases, only JHDM3/JMJD2 has been shown to act as a dual demethylase, targeting both H3K9 and H3K36 and functioning as a transcriptional repressor of the ASCL2 gene, although the consequence of simultaneous methylation of these sites remains unclear (Klose et al. 2006b; Whetstine et al. 2006). We therefore propose that KDM7 functions as an eraser of silencing marks on chromatin to unlock gene silencing. Consistent with this notion, we found that removal of methyl groups from H3K9 and H3K27 by KDM7 is associated with transcriptional activation of the follistatin gene. KDM7 belongs to the subfamily of JmjC domain-containing proteins composed of PHF2 and PHF8 in addition to KDM7. The expression of *Phf2* is concentrated in the embryonic neural tube and

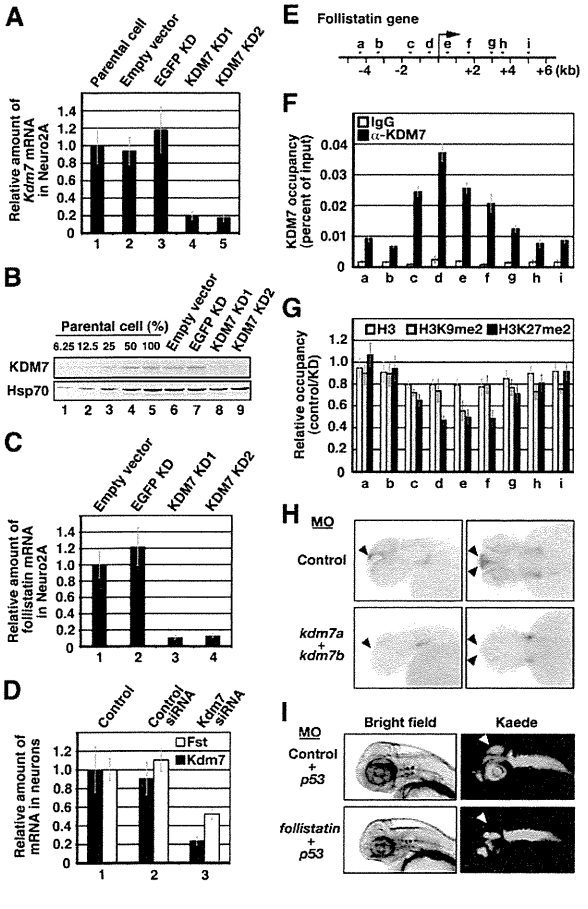

Figure 4. KDM7 directly regulates transcription and both H3K9me2 and H3K27me2 levels of the mouse follistatin gene. (*A*) Quantitative RT–PCR analysis of *Kdm7* mRNA in Neuro2A cell lines stably transfected with vectors for one of two KDM7 shRNAs (KD1 or KD2), with a vector for a control (EGFP) shRNA, or with the empty vector. The amount of *Kdm7* mRNA was normalized by that of *Gapdh* mRNA, and the normalized values are presented relative to that for the parental cells. Data are means ± SD. (*B*) Immunoblot analysis of KDM7 and Hsp70 (loading control) in the cell lines described in *A*. (*C*) Quantitative RT–PCR analysis of follistatin mRNA in the cell lines described in *A*. The amount of follistatin mRNA was normalized by that of *Gapdh* mRNA, and the normalized values are presented relative to that for the cells transfected with the empty vector. Data are means ± SD. (*D*) Quantitative RT–PCR analysis of *Kdm7* and follistatin (*Fst*) mRNAs in primary cultured mouse neurons treated with control or *Kdm7* siRNAs. The amounts of *Kdm7* and follistatin mRNAs were normalized by that of *Gapdh* mRNA, and the normalized values are presented relative to that for control cells. Data are means ± SD. (*E*) Schematic representation of the mouse follistatin genomic locus. The region from a to i was analyzed by ChIP experiments. The transcription start site is indicated by the arrow. (*F,G*) ChIP analysis of the relative occupancy of the sites in the follistatin genomic region indicated in *E* with KMD7 (*F*), as well as with H3 (white bars), H3K9me2 (gray bars), and H3K27me2 (black bars) (*G*). The analysis was performed with cells stably transfected with the vector for EGFP shRNA (control) and with cells stably expressing the KD1 shRNA for KDM7 (KD), and the results are presented as the percent of input for control cells (*F*) or the control/KD ratio (*G*). All data are means ± SD. (*H*) In situ hybridization of whole-mount zebrafish embryos at 48 hpf with an antisense follistatin RNA probe. Arrowheads indicate regions expressing the follistatin gene in embryos injected at the one-cell stage with antisense MOs for *kdm7a* (5 ng) and *kdm7b* (5 ng) or with a control MO (10 ng). (*I*) The Tg(*HuC:Kaede*) embryos were injected at the one-cell stage with antisense MOs for follistatin (5 ng) or p53 (5 ng) genes or with a control MO (5 ng) in the indicated combinations. The morphology of the embryos at 48 hpf was examined by bright-field (*left* panels) or fluorescence (*right* panels) microscopy. Arrowheads indicate the tectum or presumptive tectal region.

root ganglia in mice, and mutation of human *PHF8* causes inherited X-linked mental retardation (Hasenpusch-Theil et al. 1999; Laumonnier et al. 2005; Abidi et al. 2007; Koivisto et al. 2007). Our results showed that KDM7 is expressed predominantly in the brain of fish and mice as well as in mammalian neuronal cells and is essential for development of the fish brain, suggesting that transcriptional regulation of the follistatin gene by KDM7 may be evolutionarily conserved. Functions in neuronal development based on their demethylase activity may thus be common to this class of JmjC domain-containing proteins.

Materials and methods

In vitro histone demethylase assays

We performed in vitro demethylation assays with the use of purified recombinant proteins and various forms of histone substrates. Demethylase activity was detected by measurement of formaldehyde release, immunoblot analysis with a series of methylation-specific antibodies (Supplemental Table S1), or matrix-assisted laser desorption ionization (MALDI)–time-of-flight (TOF) mass spectrometry, as detailed in the Supplemental Material.

In situ hybridization

Whole-mount zebrafish embryos were subjected to in situ hybridization under standard conditions with digoxigenin-labeled antisense RNA probes prepared from zebrafish *kdm7a* (XM_687822), *kdm7b* (XM_681621), or follistatin 1 (DQ317968) genes.

Other methods

Details of other procedures are provided in the Supplemental Material.

Acknowledgments

We thank B.D. Strahl for providing pCAL-SpSet2, National BioResource Project ZEBRAFISH for providing *HuC:Kaede* transgenic fish, and members of our laboratories for discussion. This work was supported in part by a grant from the Ministry of Education, Culture, Sports, Science, and Technology of Japan.

References

Abidi FE, Miano MG, Murray JC, Schwartz CE. 2007. A novel mutation in the PHF8 gene is associated with X-linked mental retardation with cleft lip/cleft palate. *Clin Genet* **72:** 19–22.

Allis CD, Berger SL, Cote J, Dent S, Jenuwien T, Kouzarides T, Pillus L, Reinberg D, Shi Y, Shiekhattar R, et al. 2007. New nomenclature for chromatin-modifying enzymes. *Cell* **131:** 633–636.

Bannister AJ, Schneider R, Kouzarides T. 2002. Histone methylation: Dynamic or static? *Cell* **109:** 801–806.

Cloos PA, Christensen J, Agger K, Helin K. 2008. Erasing the methyl mark: Histone demethylases at the center of cellular differentiation and disease. *Genes & Dev* **22:** 1115–1140.

Hasenpusch-Theil K, Chadwick BP, Theil T, Heath SK, Wilkinson DG, Frischauf AM. 1999. PHF2, a novel PHD finger gene located on human chromosome 9q22. *Mamm Genome* **10:** 294–298.

Hemmati-Brivanlou A, Kelly OG, Melton DA. 1994. Follistatin, an antagonist of activin, is expressed in the Spemann organizer and displays direct neuralizing activity. *Cell* **77:** 283–295.

Iwase S, Lan F, Bayliss P, de la Torre-Ubieta L, Huarte M, Qi HH, Whetstine JR, Bonni A, Roberts TM, Shi Y. 2007. The X-linked mental retardation gene SMCX/JARID1C defines a family of histone H3 lysine 4 demethylases. *Cell* **128:** 1077–1088.

Klose RJ, Kallin EM, Zhang Y. 2006a. JmjC-domain-containing proteins and histone demethylation. *Nat Rev Genet* **7:** 715–727.

Klose RJ, Yamane K, Bae Y, Zhang D, Erdjument-Bromage H, Tempst P, Wong J, Zhang Y. 2006b. The transcriptional repressor JHDM3A demethylates trimethyl histone H3 lysine 9 and lysine 36. *Nature* **442:** 312–316.

Koivisto AM, Ala-Mello S, Lemmela S, Komu HA, Rautio J, Jarvela I. 2007. Screening of mutations in the PHF8 gene and identification of a novel mutation in a Finnish family with XLMR and cleft lip/cleft palate. *Clin Genet* **72:** 145–149.

Lachner M, O'Sullivan RJ, Jenuwein T. 2003. An epigenetic road map for histone lysine methylation. *J Cell Sci* **116:** 2117–2124.

Lan F, Nottke AC, Shi Y. 2008. Mechanisms involved in the regulation of histone lysine demethylases. *Curr Opin Cell Biol* **20:** 316–325.

Laumonnier F, Holbert S, Ronce N, Faravelli F, Lenzner S, Schwartz CE, Lespinasse J, Van Esch H, Lacombe D, Goizet C, et al. 2005. Mutations in PHF8 are associated with X linked mental retardation and cleft lip/cleft palate. *J Med Genet* **42:** 780–786.

Lin SY, Morrison JR, Phillips DJ, de Kretser DM. 2003. Regulation of ovarian function by the TGF-β superfamily and follistatin. *Reproduction* **126:** 133–148.

Margueron R, Trojer P, Reinberg D. 2005. The key to development: Interpreting the histone code? *Curr Opin Genet Dev* **15:** 163–176.

Martin C, Zhang Y. 2005. The diverse functions of histone lysine methylation. *Nat Rev Mol Cell Biol* **6:** 838–849.

Robu ME, Larson JD, Nasevicius A, Beiraghi S, Brenner C, Farber SA, Ekker SC. 2007. p53 activation by knockdown technologies. *PLoS Genet* **3:** e78. doi: 10.1371/journal.pgen.0030078.

Sato T, Takahoko M, Okamoto H. 2006. HuC:Kaede, a useful tool to label neural morphologies in networks in vivo. *Genesis* **44:** 136–142.

Shi Y, Whetstine JR. 2007. Dynamic regulation of histone lysine methylation by demethylases. *Mol Cell* **25:** 1–14.

Shi Y, Lan F, Matson C, Mulligan P, Whetstine JR, Cole PA, Casero RA, Shi Y. 2004. Histone demethylation mediated by the nuclear amine oxidase homolog LSD1. *Cell* **119:** 941–953.

Strahl BD, Allis CD. 2000. The language of covalent histone modifications. *Nature* **403:** 41–45.

Tsukada Y, Fang J, Erdjument-Bromage H, Warren ME, Borchers CH, Tempst P, Zhang Y. 2006. Histone demethylation by a family of JmjC domain-containing proteins. *Nature* **439:** 811–816.

Whetstine JR, Nottke A, Lan F, Huarte M, Smolikov S, Chen Z, Spooner E, Li E, Zhang G, Colaiacovo M, et al. 2006. Reversal of histone lysine trimethylation by the JMJD2 family of histone demethylases. *Cell* **125:** 467–481.

Zhu CC, Boone JQ, Jensen PA, Hanna S, Podemski L, Locke J, Doe CQ, O'Connor MB. 2008. *Drosophila* Activin- and the Activin-like product Dawdle function redundantly to regulate proliferation in the larval brain. *Development* **135:** 513–521.

nature cell biology

CHD8 suppresses p53-mediated apoptosis through histone H1 recruitment during early embryogenesis

Masaaki Nishiyama[1,2], Kiyotaka Oshikawa[1,2], Yu-ichi Tsukada[1,2], Tadashi Nakagawa[1,2], Shun-ichiro Iemura[3], Tohru Natsume[3], Yuhong Fan[4,5], Akira Kikuchi[6], Arthur I. Skoultchi[4] and Keiichi I. Nakayama[1,2,7]

The chromodomain helicase DNA-binding (CHD) family of enzymes is thought to regulate gene expression, but their role in the regulation of specific genes has been unclear. Here we show that CHD8 is expressed at a high level during early embryogenesis and prevents apoptosis mediated by the tumour suppressor protein p53. CHD8 was found to bind to p53 and to suppress its transactivation activity. CHD8 promoted the association of p53 and histone H1, forming a trimeric complex on chromatin that was required for inhibition of p53-dependent transactivation and apoptosis. Depletion of CHD8 or histone H1 resulted in p53 activation and apoptosis. Furthermore, *Chd8*$^{-/-}$ mice died early during embryogenesis, manifesting widespread apoptosis, whereas deletion of *p53* ameliorated this developmental arrest. These observations reveal a mode of p53 regulation mediated by CHD8, which may set a threshold for induction of apoptosis during early embryogenesis by counteracting p53 function through recruitment of histone H1.

Although apoptosis has a key role in organization of the developing embryo, it is not fully understood how apoptosis is regulated during embryogenesis. The tumour suppressor protein p53 mediates the induction of apoptosis in response to DNA damage caused by genotoxic stress. It activates the transcription of numerous genes, and thereby triggers cell-cycle arrest, senescence or apoptosis to prevent tumorigenesis[1–5].

Activation of transcription by p53 is regulated, at least in part, by the amount of p53 as well as by post-translational modifications of p53 (refs 6–8). In addition, certain chromatin-associated proteins that change chromatin configuration interact with p53 and thereby modulate its transactivation activity[5,9–12]. Although these findings suggest that chromatin configuration may affect the transactivation activity of p53, the mechanism by which the structure of chromatin changes, as well as the biological outcome of such regulation, have remained largely unknown.

Certain classes of molecules recognize modified histones and are thought to translate the modification code into specific functions. Such proteins include members of the chromodomain helicase DNA-binding (CHD) family of enzymes, which also belong to the SNF2 superfamily of ATP-dependent chromatin remodellers[13–15]. Chd1 of *Saccharomyces cerevisiae* is a component of the multi-subunit histone acetyltransferase complexes SAGA and SLIK[16], and is required for methylation of histone H3 at Lys 4 (H3K4; ref. 17). Human CHD1 catalyses the ATP-dependent transfer of histones from the NAP-1 chaperone to DNA, resulting in the assembly of active chromatin[18,19]. Nine genes for CHD1-related proteins have been identified in mammalian species.

Among these proteins, CHD8 (Duplin) was originally isolated as a negative regulator of the Wnt–β-catenin signalling pathway[20]. The carboxy-terminal region of CHD8 interacts with the insulator-binding protein CTCF, and this interaction is important for insulator activity[21]. We previously generated *Chd8*$^{-/-}$ mice and showed that these animals die *in utero* between embryonic day (E) 5.5 and E7.5, manifesting widespread apoptosis[22]. However, Wnt activation was not seen in the *Chd8*$^{-/-}$ embryos before their death. Although these observations suggest that CHD8 may possess anti-apoptotic activity that is independent of Wnt signalling inhibition, it has been unclear how the loss of CHD8 induces apoptosis. We now show that CHD8 binds to both p53 and histone H1, and that these interactions facilitate recruitment of histone H1 to p53 target genes, resulting in suppression of their expression and of apoptosis induced by genotoxic insults. These results thus suggest that loss of CHD8 in mice induces apoptosis as a result of unrestrained p53 activity at the early stage of embryonic development. Consistent with this conclusion, deletion of *p53* in *Chd8*$^{-/-}$ mice ameliorated the developmental arrest. The physiological role of CHD8 may thus be to prevent such unwanted apoptosis during early embryogenesis.

[1]Department of Molecular and Cellular Biology, Medical Institute of Bioregulation, Kyushu University, 3-1-1 Maidashi, Higashi-ku, Fukuoka, Fukuoka 812-8582, Japan. [2]CREST, Japan Science and Technology Agency (JST), Kawaguchi, Saitama 332-0012, Japan. [3]National Institute of Advanced Industrial Science and Technology (AIST), Biological Information Research Center (JBIRC), Kohtoh-ku, Tokyo 135-0064, Japan. [4]Department of Cell Biology, Albert Einstein College of Medicine, 1300 Morris Park Avenue, Bronx, NY 10461, USA. [5]School of Biology and the Petit Institute for Bioengineering and Bioscience, Georgia Institute of Technology, IBB 2313, 315 Ferst Drive, Atlanta, GA 30332-0363, USA. [6]Department of Biochemistry, Graduate School of Biomedical Sciences, Hiroshima University, 1-2-3 Kasumi, Minami-ku, Hiroshima 734-8551, Japan.
[7]Correspondence should be addressed to K.I.N. (e-mail: nakayak1@bioreg.kyushu-u.ac.jp)

Received 29 July 2008; accepted 28 October 2008; published online 18 January 2009; DOI: 10.1038/ncb1831

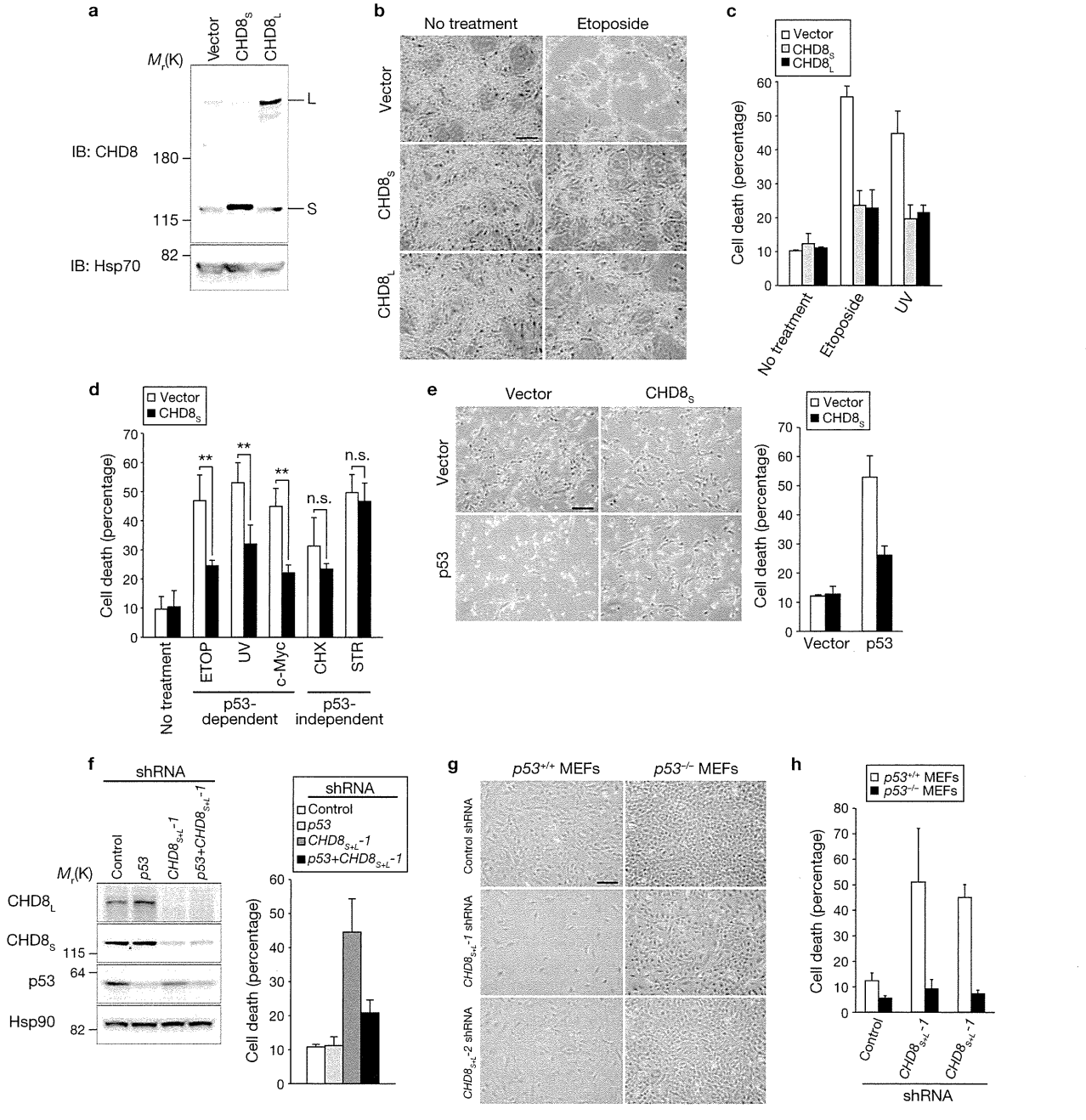

Figure 1 Anti-apoptotic activity of CHD8. (**a–c**) NIH 3T3 cells overexpressing $CHD8_S$ or $CHD8_L$ were subjected to immunoblot (IB, **a**) analysis with anti-CHD8 and exposed to genotoxic stress. Cells were examined by phase-contrast microscopy (**b**) and the percentage of dead cells was determined by trypan blue staining (**c**). Data in **c** are mean ± s.d., $n = 3$. (**d**) NIH 3T3 cells overexpressing $CHD8_S$ were exposed to etoposide (ETOP, 50 μM), cycloheximide (CHX, 100 μg ml^{-1}), staurosporine (STR, 1 μM), UV radiation or c-Myc overexpression. Data in **d** are mean ± s.d., $n = 3$ (** $P < 0.01$; n.s., not significant; $P > 0.05$; Student's *t*-test). (**e**) U2OS cells were infected with retroviral vectors for $CHD8_S$ or p53 and were stained with trypan blue (left panel). Data shown in the right panel are mean ± s.d., $n = 3$. (**f**) U2OS cells were infected with retroviral vectors encoding shRNAs specific for *p53*, both $CHD8_S$ and $CHD8_L$ ($CHD8_{S+L}$-*1*) or *EGFP* (control), subjected to immunoblotting (left panel), stained with trypan blue and the percentage of dead cells determined (right panel). Data shown in the right panel are mean ± s.d., $n = 3$. (**g**, **h**) $p53^{+/+}$ or $p53^{-/-}$ MEFs infected with retroviral vectors for $CHD8_{S+L}$-*1* or $CHD8_{S+L}$-*2* shRNAs were examined by phase-contrast microscopy (**g**) and the percentage of dead cells determined by trypan blue staining (**h**). Data in **h** are mean ± s.d., $n = 3$. Scale bars are 100 μm (**b**, **e**, **g**).

RESULTS

CHD8 suppresses p53-dependent apoptosis

Mouse *Chd8* consists of 37 exons spanning about 40 kb. Alternative splicing of exon 9 generates two transcripts that encode a protein ($CHD8_L$) with a relative molecular mass of 280,000 (M_r 280K), containing two chromodomains (a helicase/ATPase domain and a DNA binding domain) and a 110K protein ($CHD8_S$, also known as Duplin), which contains only the amino-terminal chromodomain (Supplementary Information, Fig. S1a, b). These molecules are expressed in most cell lines and tissues (Supplementary Information, Fig. S1c, d), but the ratio of $CHD8_L$ to $CHD8_S$ varies.

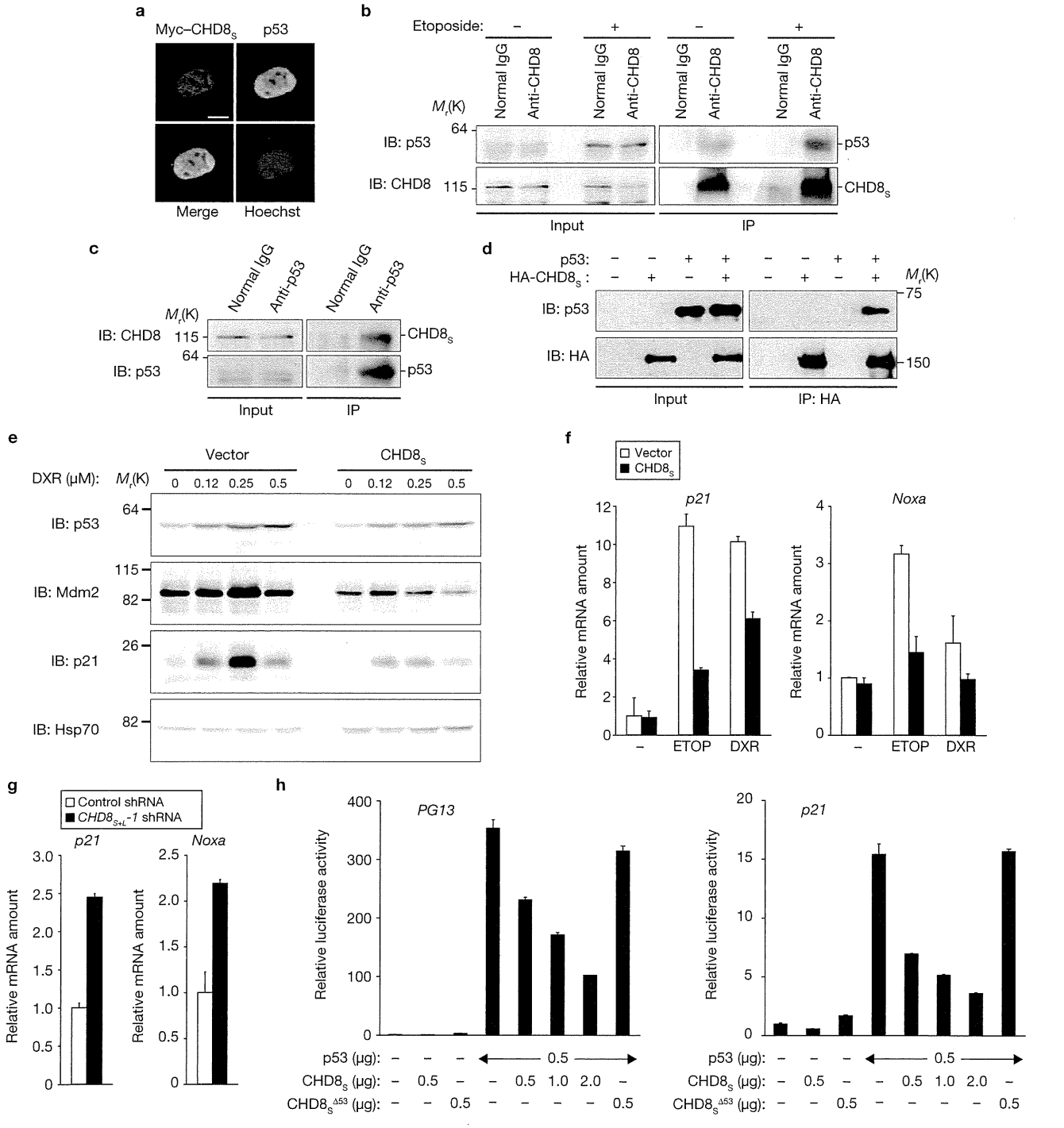

Figure 2 CHD8 interacts with and inhibits transactivation by p53. (**a**) HeLa cells expressing Myc–$CHD8_S$ were immunostained with anti-Myc or p53. Scale bar, 5 μm. (**b**) U2OS cells were incubated with etoposide and then subjected to immunoprecipitation (IP) with an anti-CHD8 antibody, and immunoblot analysis with an anti-p53 antibody. (**c**) Immunoprecipitation of U2OS lysates with anti-p53 and immunoblot analysis with an anti-CHD8 antibodies. (**d**) *In vitro* binding assay for recombinant $CHD8_S$ and p53. (**e**) U2OS cells overexpressing $CHD8_S$ were incubated with doxorubicin (DXR) and then subjected to immunoblot analysis with the indicated antibodies. (**f**) U2OS cells overexpressing $CHD8_S$ were treated with the genotoxic agents DXR (0.5 μM) and etoposide (ETOP, 20 μM) and then subjected to qRT–PCR. (**g**) U2OS cells infected with a retroviral vector encoding *$CHD8_{S+L}$-1* shRNA were subjected to qRT–PCR. (**h**) Luciferase assay using either wild-type or mutant $CHD8_S^{\Delta 53}$. Data are mean ± s.d., $n = 3$ (**f**–**h**).

Given that lack of both $CHD8_S$ and $CHD8_L$ results in widespread apoptosis in mouse embryos[22], we hypothesized that CHD8 may possess anti-apoptotic activity. Indeed, overexpression of either $CHD8_S$ or $CHD8_L$ inhibited the induction of apoptosis in mouse NIH 3T3 cells exposed to etoposide or ultraviolet (UV) radiation (Fig. 1a–c; Supplementary Information, Fig. S2a). The apoptosis-related cleavage of both caspase-3 and poly(ADP-ribose) polymerase (PARP) was also inhibited by overexpression of CHD8

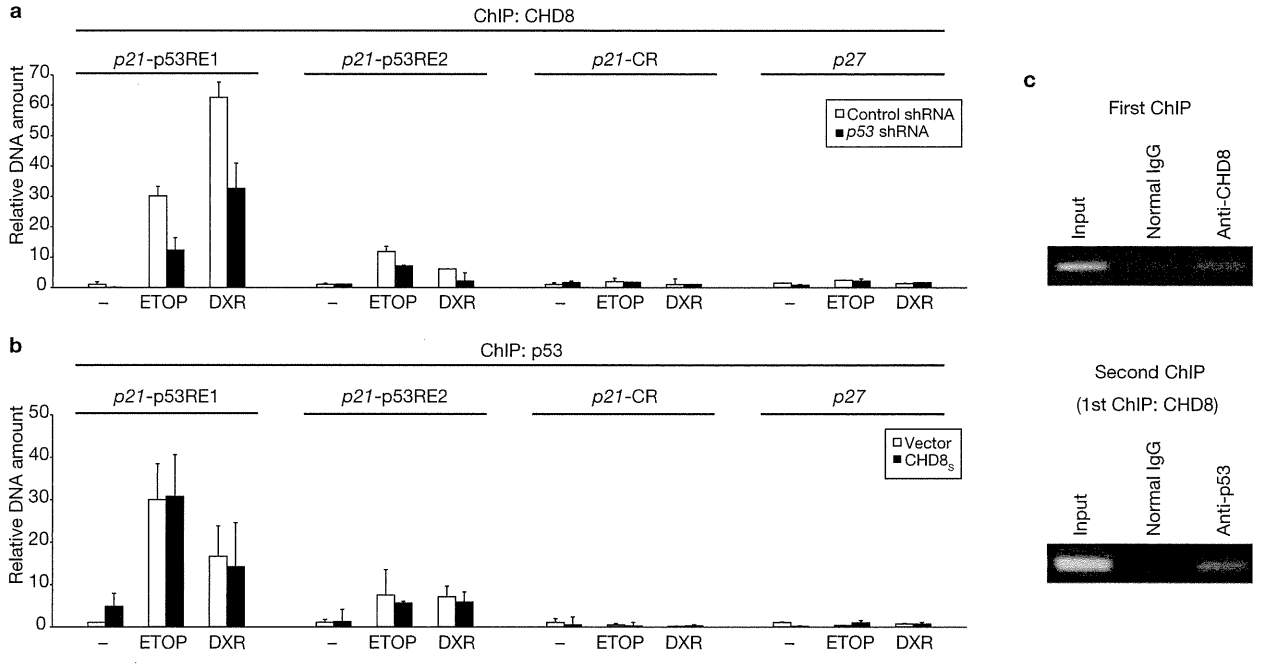

Figure 3 CHD8 binds to the promoters of p53 target genes. (**a**) U2OS cells infected with a retroviral vector encoding *p53* shRNA were incubated with the genotoxic agents etoposide (ETOP, 20 μM) and doxorubicin (DXR, 0.5 μM). The cells were then subjected to ChIP with an anti-CHD8 antibody and the precipitated DNA was quantified by real-time PCR with primers specific for p53-responsive elements (p53REs) 1 or 2 or a control region (CR) of the *p21* promoter or for the *p27* promoter. (**b**) U2OS cells overexpressing $CHD8_S$ were treated with ETOP (20 μM) and DXR (0.5 μM) and subjected to ChIP with an anti-p53 antibody. Data are mean ± s.d., $n = 3$ (**a**, **b**). (**c**) U2OS cells overexpressing $CHD8_S$ were incubated with ETOP and then subjected to ChIP with an anti-CHD8 antibody. The immunoprecipitates were subjected to ChIP with an anti-p53 antibody.

(Supplementary Information, Fig. S2b). CHD8 markedly suppressed apoptosis induced by etoposide, UV radiation or c-Myc, all of which are dependent on p53, but did not affect apoptosis induced by cycloheximide or staurosporine, which are independent of p53 (Fig. 1d). Furthermore, apoptosis induced by overexpression of p53 was inhibited by $CHD8_S$ (Fig. 1e) or $CHD8_L$ (Supplementary Information, Fig. S3a).

Conversely, depletion of both $CHD8_S$ and $CHD8_L$ by RNA interference (RNAi) induced cell death in U2OS human osteosarcoma cells (Fig. 1f), which harbour wild-type *p53* alleles, as well as in HeLa and HCT116 cells (Supplementary Information, Fig. S3b–d). Depletion of $CHD8_L$ alone had no such effect. We confirmed that cell death triggered by depletion of CHD8 is due to apoptosis (Supplementary Information, Fig. S2c, d). Together, these observations indicate that both $CHD8_S$ and $CHD8_L$ possess anti-apoptotic activity and that the presence of $CHD8_S$ alone in cells is sufficient to prevent apoptosis, suggesting that the anti-apoptotic activity of CHD8 is dependent on the common region of $CHD8_S$ and $CHD8_L$. Apoptosis induced by depletion of CHD8 was blocked by the caspase inhibitor Z-VAD–fmk and was associated with retardation of cell growth (Supplementary Information, Fig. S2e, f).

To investigate whether the apoptosis induced by CHD8 depletion was dependent on p53, we depleted U2OS cells of both CHD8 and p53 and found that additional depletion of p53 in cells depleted of CHD8 restored cell survival (Fig. 1f). Depletion of CHD8 resulted in a marked increase in apoptosis in $p53^{+/+}$ MEFs, but had virtually no effect in $p53^{-/-}$ MEFs (Fig. 1g, h), indicating that CHD8 depletion results in p53 activation. These data thus indicate that CHD8 is an anti-apoptotic molecule and a negative regulator of p53.

CHD8 interacts with and inhibits p53

The subcellular localization of $CHD8_S$ was found to be almost identical to that of p53, with both proteins being largely restricted to the nucleus (Fig. 2a). Reciprocal co-immunoprecipitation analysis revealed that endogenous CHD8 specifically interacted with endogenous p53 in U2OS cells (Fig. 2b, c; Supplementary Information, Fig. S3e). Similar experiments with a series of deletion mutants of $CHD8_S$ revealed that the N-terminal region of CHD8 is responsible for binding to p53 (Supplementary Information, Fig. S4a). Reciprocal analysis showed that CHD8 binds to the central core domain of p53 (Supplementary Information, Fig. S4b). Furthermore, pulldown assays revealed that recombinant $CHD8_S$ and recombinant p53 bound to each other *in vitro*, suggesting that the interaction is direct (Fig. 2d).

We next examined whether CHD8 affects transcriptional activation by p53 in U2OS cells. Overexpression of $CHD8_S$ or $CHD8_L$ markedly inhibited the etoposide- or doxorubicin-induced upregulation of Mdm2, p21 and Noxa, all of which are encoded by p53 target genes, in U2OS cells (Fig. 2e, f; Supplementary Information, Figs S3f, S5a–c). In contrast, depletion of CHD8 resulted in an increase in the expression of p53 target genes, including those for *p21* and *Noxa* (Fig. 2g), suggesting that CHD8 antagonizes p53 function. Furthermore, overexpression of $CHD8_S$ inhibited in a concentration-dependent manner the p53-induced increase in luciferase activity in human osteosarcoma SaOS2 cells (*p53*-null) harbouring a *luciferase* gene fused to the promoter of the p53 target genes for *p21* or *PG13* (Fig. 2h). $CHD8_S$ overexpression did not affect the activity of a *p21* promoter in which the two p53 binding sites are mutated (Supplementary Information, Fig. S5d). The inhibitory effect of $CHD8_S$ was not mimicked by the $CHD8_S^{\Delta 53}$ mutant (Fig. 2h; Supplementary Information, Fig. S5d), which lacks

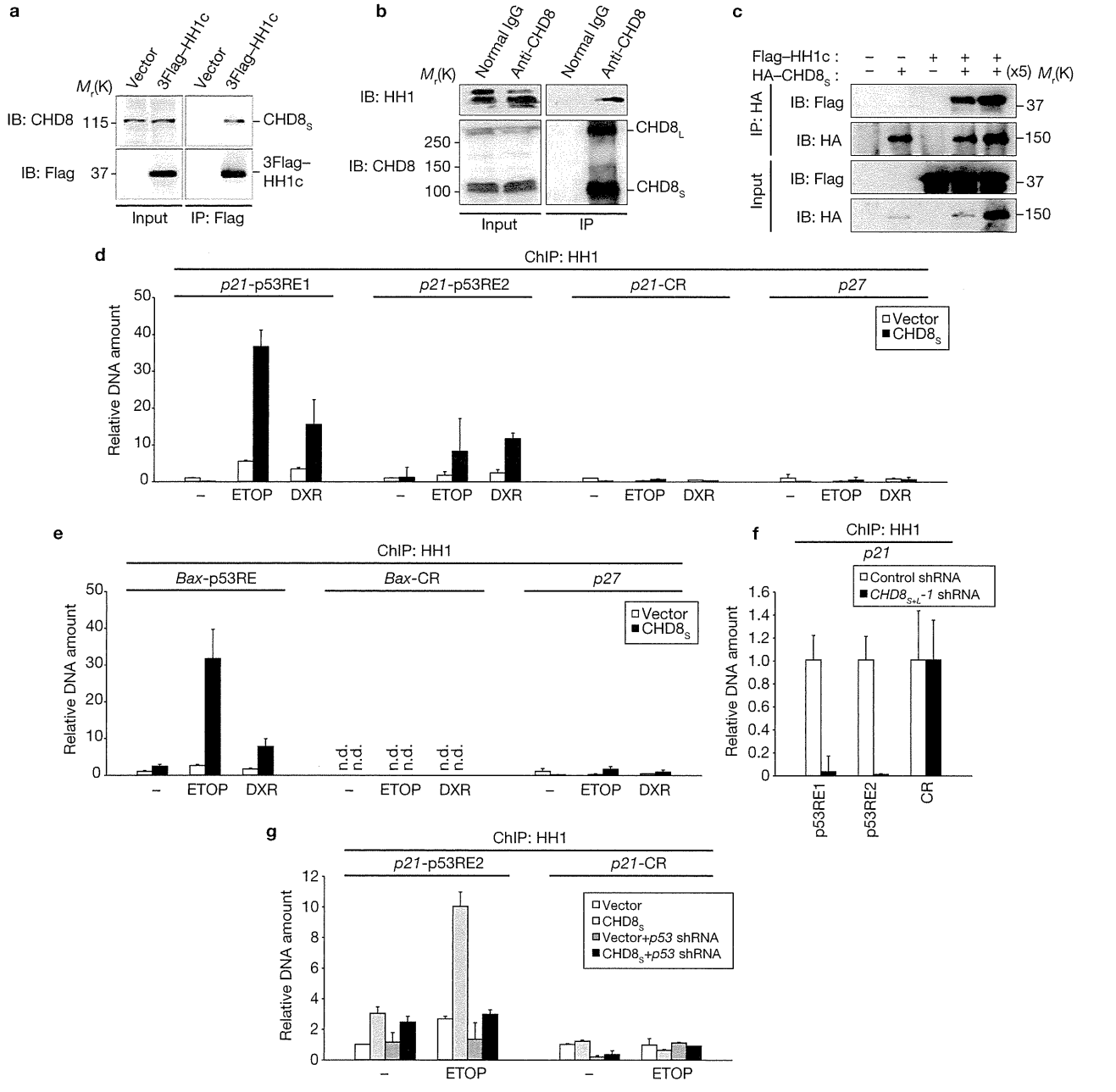

Figure 4 CHD8 recruits histone H1 to the promoters of p53 target genes. (**a**) HEK293T cells expressing 3 × Flag–histone H1c were subjected to immunoprecipitation with anti-Flag and immunoblot analysis with anti-CHD8 antibodies. (**b**) Immunoprecipitation of HEK293T lysates with anti-CHD8 and immunoblot analysis with anti-histone H1 antibodies. (**c**) *In vitro* binding assay for recombinant CHD8$_S$ and histone H1c. (**d**) U2OS cells overexpressing CHD8$_S$ were treated with the genotoxic agents etoposide (ETOP, 20 μM) and doxorubicin (DXR, 0.5 μM) and subjected to ChIP with an anti-histone H1 antibody. (**e**) ChIP was performed for the *BAX* promoter (n.d., not detected). (**f**) U2OS cells infected with a retroviral vector for *CHD8$_{S+L}$-1* shRNA were subjected to ChIP. (**g**) U2OS cells overexpressing CHD8$_S$ were infected with a retroviral vector for *p53* shRNA, incubated with ETOP and then subjected to ChIP. Data are mean ± s.d., $n = 3$ (**d–g**).

the p53-binding domain (Supplementary Information, Fig. S5e), suggesting that binding of CHD8 to p53 is required for suppression of p53 function. CHD8$_S$ did not affect the activity of the transcription factor NF-κB induced by TRAF2 (Supplementary Information, Fig. S5f), suggesting that it is not a general inhibitor of transcription but rather, a specific inhibitor of p53-dependent transactivation. Together, these data indicate that CHD8 interacts with p53 and thereby negatively regulates its function.

CHD8 recruits histone H1 to inhibit p53

We next investigated the possible association of CHD8 and p53 with the promoter regions of p53 target genes using chromatin immunoprecipitation (ChIP; Supplementary Information, Fig. S6). ChIP using anti-CHD8 antibodies revealed that CHD8 specifically associated with p53-responsive elements 1 and 2 of the *p21* promoter in U2OS cells treated with etoposide or doxorubicin but not in untreated cells (Fig. 3a). No substantial association of CHD8 with a control region of the *p21*

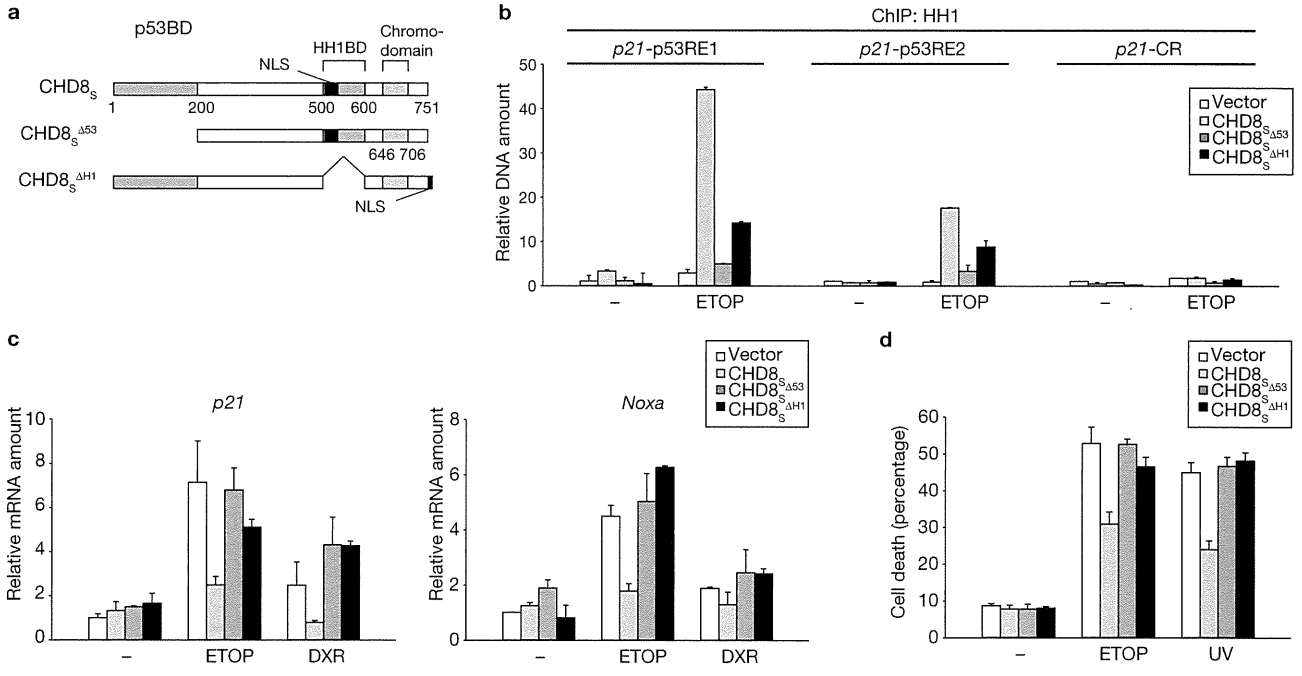

Figure 5 Interaction of CHD8 with p53 and histone H1 is necessary for recruitment of histone H1 to the promoters of p53 target genes. (**a**) Schematic representation of $CHD8_S$ derivatives. (**b–d**) U2OS cells overexpressing $CHD8_S$ derivatives were exposed to genotoxic stress (etoposide, ETOP, 20 μM and doxorubicin, DXR, 0.5 μM) and then subjected to ChIP (**b**), qRT–PCR (**c**) and trypan blue staining (**d**). Data are mean ± s.d., $n = 3$.

promoter that does not bind p53 or with the *p27* promoter was detected. Moreover, depletion of *p53* by RNAi reduced the extent of CHD8 association with the p53-responsive elements of the *p21* promoter, suggesting that p53 mediates the association of CHD8 with chromatin. ChIP using anti-p53 antibodies revealed that $CHD8_S$ overexpression did not affect the association of p53 with chromatin in response to genotoxic stress (Fig. 3b), suggesting that p53 binds to the *p21* promoter in a CHD8-independent manner. A sequential ChIP experiment revealed that p53 and CHD8 occupy the *p21* promoter region simultaneously (Fig. 3c).

To elucidate the mechanism by which CHD8 inhibits p53 function, we attempted to identify molecules that associate with Flag–$CHD8_S$ in HEK293T cells using a 'shotgun' proteomics approach. The results of several independent experiments revealed that histone H1 was consistently the most prominent of the proteins associated with immunoprecipitated Flag–$CHD8_S$ (Supplementary Information, Table S1). Reciprocal co-immunoprecipitation analysis showed that Flag-tagged histone H1c interacted with endogenous CHD8 (Fig. 4a). We also confirmed that endogenous CHD8 associated with endogenous histone H1 (Fig. 4b). Furthermore, pulldown assays revealed that recombinant $CHD8_S$ and recombinant histone H1c bound to each other *in vitro*, suggesting that the interaction is direct (Fig. 4c). We examined which histone H1 subtypes interact with CHD8 in a co-immunoprecipitation assay. This analysis revealed that all five major H1 subtypes (H1a, H1b, H1c, H1d, H1e) interacted with $CHD8_S$ (Supplementary Information, Fig. S4c). *In vitro* binding assays with a series of deletion mutants showed that residues 500–600 is the region of $CHD8_S$ required for binding to histone H1 (Supplementary Information, Fig. S4d). The histone H1-binding domain thus includes the nuclear localization signal of $CHD8_S$ and is distinct from the chromodomain at the C terminus.

Given that CHD8 was found to interact with histone H1, we also examined whether histone H1 is recruited to the p53-responsive elements of the *p21* promoter. ChIP using an anti–histone H1 antibody showed that histone H1 was indeed recruited to the *p21* promoter on treatment of U2OS cells with etoposide or doxorubicin, and this effect was markedly enhanced by overexpression of $CHD8_S$ (Fig. 4d). Similar results were obtained with the promoter of the p53 target gene *BAX* (Fig. 4e). Conversely, depletion of either CHD8 or p53 markedly reduced the amount of histone H1 associated with the *p21* promoter (Fig. 4f, g). This series of ChIP experiments thus suggests that a p53–CHD8–histone H1 complex forms at the promoters of p53-inducible genes in response to genotoxic stress.

p53–CHD8–histone H1 complex is necessary for suppression of p53 function

We next examined the ability of CHD8 mutants that lack either the p53 binding domain ($CHD8_S^{\Delta 53}$) or the histone H1 binding domain ($CHD8_S^{\Delta H1}$) to recruit histone H1 to the promoters of p53 target genes (Fig. 5a). Given that the $CHD8_S^{\Delta H1}$ mutant lacks residues 500–600, which include the nuclear localization signal, we added the nuclear localization signal of the large T antigen of simian virus 40 to the C terminus of the mutant protein. Deletion of either of the two binding domains markedly impaired the ability of $CHD8_S$ to recruit histone H1 to the p53-responsive elements of the *p21* promoter (Fig. 5b). Furthermore, neither $CHD8_S^{\Delta 53}$ nor $CHD8_S^{\Delta H1}$ had an inhibitory effect on p53-dependent transactivation (Fig. 5c) or apoptosis (Fig. 5d). Together, these data suggest that CHD8 recruits histone H1 to p53-responsive elements, and that such recruitment of histone H1 results in suppression of transcriptional activation by p53.

Histone H1 is essential for repression of p53-dependent transcription

Our observation that the $CHD8_S^{\Delta H1}$ mutant is unable to repress p53 function led us to investigate the requirement for histone H1 in such repression. To this end, we adopted three independent approaches.

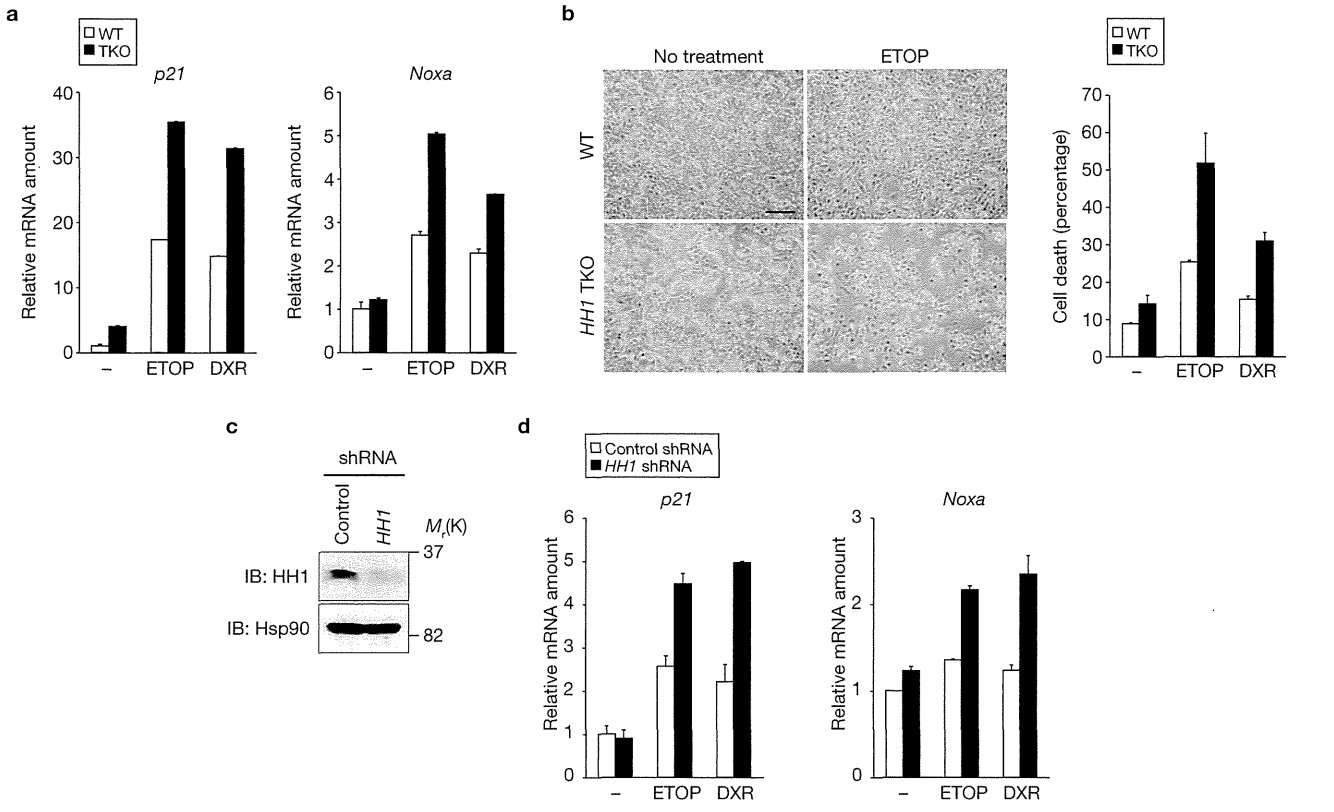

Figure 6 Requirement for histone H1 in repression of p53-mediated transcription. (**a**, **b**) Wild-type (WT) or *HH1c*$^{-/-}$*HH1d*$^{-/-}$*HH1e*$^{-/-}$ triple-knockout (TKO) ES cells were incubated with etoposide (ETOP, μ2 M) and doxorubicin (DXR, 0.05 μM) and then subjected to qRT–PCR (**a**) and trypan blue staining (**b**). (**c**) U2OS cells were infected with a retroviral vector for *histone H1* (*HH1*) shRNA and then subjected to immunoblot analysis. (**d**) The cells were incubated with ETOP (2 μM) and DXR (0.05 μM) and then subjected to qRT–PCR. Data are mean ± s.d., $n = 3$ (**a**, **b**, **d**).

First, CHD8-dependent suppression of p53 function was examined in *HH1c*$^{-/-}$*HH1d*$^{-/-}$*HH1e*$^{-/-}$ triple-knockout (TKO) embryonic stem (ES) cells[23]. Expression of *p21* and *Noxa* genes (Fig. 6a), as well as the level of apoptosis (Fig. 6b) induced by genotoxic stress, were markedly increased in TKO cells, compared with those in control cells. Second, U2OS cells were subjected to RNAi with a short hairpin RNA (shRNA) designed to deplete all five major subtypes of histone H1 (Fig. 6c). Such depletion of histone H1 resulted in a substantial increase in etoposide- or doxorubicin-induced upregulation of *p21* or *Noxa* mRNA levels (Fig. 6d). Third, expression of a dominant-negative mutant of histone H1 (N-fusion) reduced the amount of endogenous histone H1, as described previously[24], and also increased that of p21, resulting in suppression of cell proliferation (Supplementary Information, Fig. S7). Expression of a histone H1 mutant that does not have dominant-negative activity (C-fusion) did not affect the abundance of p21 or cell proliferation. Together, these three lines of evidence support our conclusion that CHD8 negatively regulates p53 function by recruiting histone H1 to the promoters of p53 target genes, resulting in suppression of apoptosis triggered by p53.

Survival of *Chd8*$^{-/-}$*p53*$^{-/-}$ embryos

The abundance of CHD8 mRNA or protein in mouse embryos was greater during early embryogenesis than at later embryonic stages or in newborns (Fig. 7a, b). In addition to mouse embryos, all human and mouse cancer cell lines tested in this study were found to express CHD8 at relatively high levels (Supplementary Information, Fig. S1c, e, f). Given that CHD8 is a negative regulator of p53, we reasoned that the early embryonic death of *Chd8*$^{-/-}$ mice may be attributable to unscheduled activation of p53. To test this hypothesis, we examined whether deletion of *p53* ameliorated the abnormalities of *Chd8*$^{-/-}$ embryos. Most of the *Chd8*$^{-/-}$ mice died *in utero* between E5.5 and E7.5 and none survived beyond E8.5, whereas *Chd8*$^{-/-}$*p53*$^{-/-}$ embryos survived until E10.5 (Supplementary Information, Table S2). Histopathological examination revealed that the growth retardation seen in *Chd8*$^{-/-}$ embryos was markedly less pronounced in *Chd8*$^{-/-}$*p53*$^{-/-}$ and *Chd8*$^{-/-}$*p53*$^{+/-}$ embryos at E7.5 and E8.5 (Fig. 7c). Cells with condensed nuclei were not seen in *Chd8*$^{-/-}$*p53*$^{-/-}$ embryos at E8.5. The extent of recovery was greater in *Chd8*$^{-/-}$*p53*$^{-/-}$ embryos than in *Chd8*$^{-/-}$*p53*$^{+/-}$ embryos, suggesting that it was related to the reduction in the amount of *p53*. Mesoderm formation, a crucial event in early embryonic development that does not occur in *Chd8*$^{-/-}$ mice, was observed in *Chd8*$^{-/-}$*p53*$^{-/-}$ mice (Fig. 7d). *Chd8*$^{-/-}$*p53*$^{-/-}$ embryos died *in utero* at E10.5 and had severe haemorrhage, indicative of a defect in the cardiovascular system (M.N and K.I.N., unpublished data), suggesting that CHD8 also has another function (or functions) that is required for mid-stage embryonic development. We also observed growth of E3.5 embryos (blastocysts) in culture. *Chd8*$^{-/-}$ blastocysts degenerated between E5.5 and E7.5, whereas *Chd8*$^{-/-}$*p53*$^{-/-}$ blastocysts, like wild-type controls, were alive at E9.5 (Fig. 7e). It is thus likely that the embryonic death of *Chd8*$^{-/-}$ mice is attributable to the unscheduled activation of p53-dependent apoptosis.

To investigate the physiological role of CHD8 during early embryogenesis, we examined embryos at various stages. In ES cells (equivalent to E3.5 embryos), endogenous CHD8 was shown to interact with both endogenous p53 (Fig. 8a) and endogenous histone H1 (Fig. 8b). Furthermore,

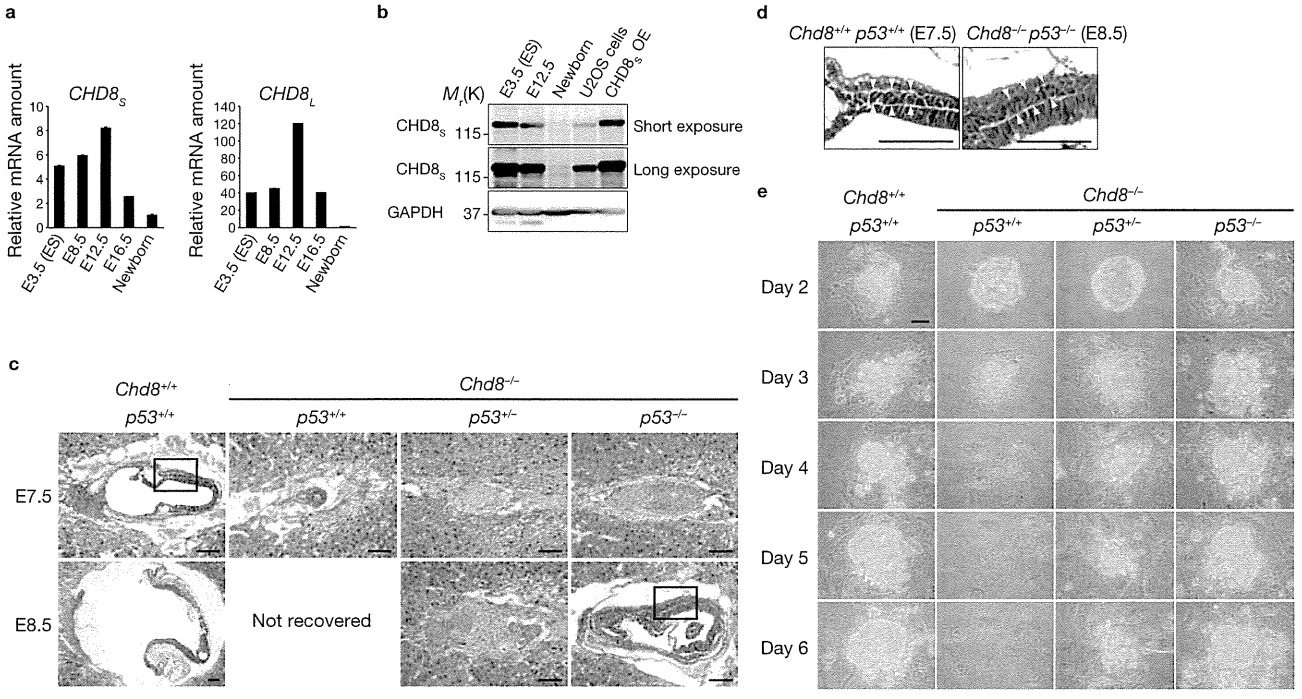

Figure 7 Deletion of *p53* rescues the phenotype of CHD8-deficient mice. (**a**) qRT–PCR for $CHD8_S$ and $CHD8_L$ mRNAs in mouse embryos at the indicated stages. Data are mean ± s.d., $n = 3$. (**b**) Immunoblot analysis of $CHD8_S$ in mouse embryos as well as in U2OS cells and those overexpressing (OE) $CHD8_S$. (**c**) Histopathological examination of $Chd8^{+/+}p53^{+/+}$, $Chd8^{-/-}p53^{+/+}$, $Chd8^{-/-}p53^{+/-}$ and $Chd8^{-/-}p53^{-/-}$ embryos stained with haematoxylin and eosin. (**d**) Higher-magnification views of the boxed regions in **c**. Arrowheads indicate a layer of mesoderm. (**e**) *In vitro* culture of blastocysts of the indicated genotypes. Scale bars are 100 μm (**c–e**).

RNAi-mediated depletion of *CHD8* promoted both apoptosis (Fig. 8c, d) and expression of the p53 target genes *p21* and *Noxa* (Fig. 8e). Cultured $Chd8^{-/-}$ blastocysts (equivalent to E5.5 embryos) also showed higher levels of *p21* and *Noxa* mRNAs than did wild-type blastocysts (Fig. 8f). In E7.5 embryos, TUNEL assay showed substantial apoptosis in $Chd8^{-/-}$ embryos, whereas no apoptosis was observed in wild-type or $Chd8^{-/-}p53^{-/-}$ embryos (Fig. 8g). Furthermore, Mdm2 expression was upregulated in $Chd8^{-/-}$ embryos in a p53-dependent manner (Fig. 8h). This genetic evidence supports the notion that CHD8 is a physiological antagonist of p53 *in vivo*, and that loss of CHD8 allows unrestrained p53 activity, which induces apoptosis at the early stage of embryonic development. We therefore propose that the biological role of CHD8 is to suppress unwanted apoptosis during early embryogenesis (Fig. 8i).

DISCUSSION

We have shown that CHD8 negatively regulates p53 function by recruiting histone H1 to the promoters of p53 target genes. Formation of the p53–CHD8–histone H1 complex requires expression of CHD8 and stabilization of p53 by genotoxic stress. CHD8 is preferentially expressed in embryonic tissues and in cancer cell lines that are thought to reflect the embryonic state. Loss of CHD8 induced hyperactivation of p53, resulting in apoptosis, which was prevented by depletion of p53. The biochemical and genetic evidence provided by our study may explain how p53 function is regulated by histone H1.

Histone modification is a fundamental mechanism for epigenetic control of gene expression. The role of core histones in gene regulation has been studied extensively, but that of the linker histone H1 has remained unclear. *In vitro* studies suggest that linker histone molecules influence chromatin structure, nucleosome mobility and gene regulation[25–32]. Histone H1 is not essential for growth or cell division in several unicellular eukaryotes[33–36], but ablation of three of eight genes that encode isoforms of histone H1 in mouse ES cells, resulting in a 50% reduction in histone H1 content, led to embryonic death of the mutant mice[23,37]. Such downregulation of histone H1 elicited marked changes in chromatin structure, including a global reduction in nucleosome spacing, local reduction in chromatin compaction and changes in the modification of core histones. Despite these changes, microarray analysis of the mutant ES cells revealed that expression of only a few genes was altered[23]. These observations suggest that histone H1 participates in the regulation of specific genes that are essential for survival.

In response to genotoxic stress, mammalian cells activate a complex network of proteins, a key element of which is p53. Post-translational modification of p53 results in transcriptional activation of its target genes[1,6,7]. Regulation of p53 by checkpoint signalling was originally thought to be mediated almost exclusively at the post-translational level[1,6,8]. More recently, p53 has also been found to be regulated at the transcriptional[38] and translational[39] levels. We have now uncovered another mode of p53 regulation mediated by CHD8-dependent recruitment of histone H1 to the promoters of its target genes.

Cells proliferate extensively with short G_1 and G_2 phases during early embryogenesis. The DNA replication checkpoint may therefore be readily activated at this time, with the consequent risk of inducing p53-dependent apoptosis. We propose that the biological role of CHD8 is to suppress unwanted apoptosis during early embryogenesis (Fig. 8i). Consistent with this notion, we found that the amounts of CHD8 mRNA and protein are higher during the early and mid phases of mouse embryonic development

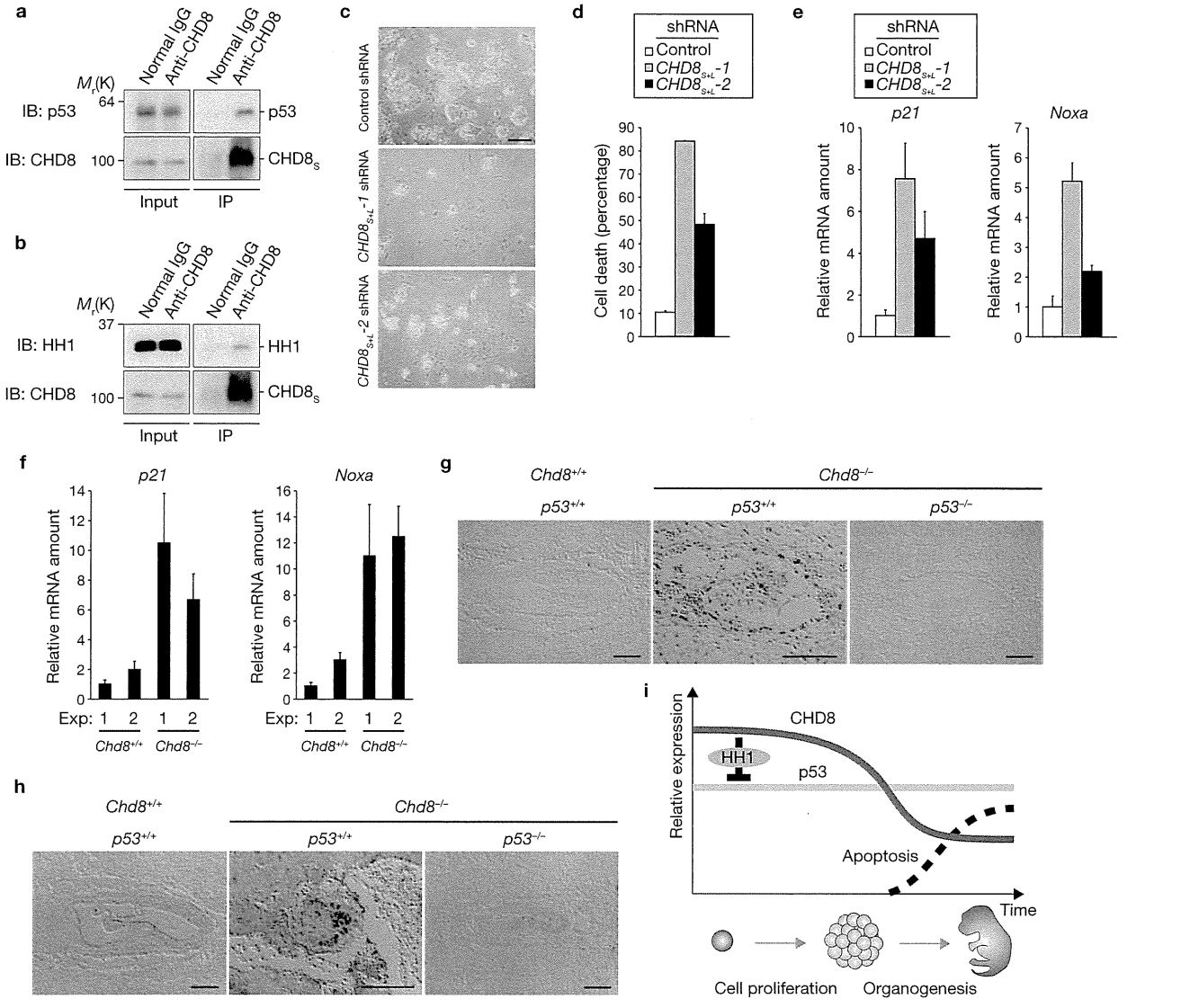

Figure 8 CHD8 sets a threshold for induction of apoptosis during early embryogenesis by counteracting p53 function. (**a**, **b**) Immunoprecipitation of ES cell lysates with an anti-CHD8 antibody, and immunoblot analysis with either anti-p53 (**a**) or anti-histone H1 (**b**) antibodies. (**c**–**e**) ES cells infected with retroviral vectors for $CHD8_{S+L}$-*1* or $CHD8_{S+L}$-*2* shRNAs were subjected to trypan blue staining (**c**, quantification shown in **d**) and qRT–PCR (**e**). (**f**) $Chd8^{+/+}$ or $Chd8^{-/-}$ blastocysts were subjected to qRT–PCR for *p21* and *Noxa*. Data are mean ± s.d., $n = 3$ (**d**–**f**). (**g**, **h**) Sections of $Chd8^{+/+}p53^{+/+}$, $Chd8^{-/-}p53^{+/+}$ and $Chd8^{-/-}p53^{-/-}$ embryos were subjected to TUNEL assay (**g**) or to immunohistochemistry (**h**) with anti-Mdm2 antibody. Scale bars are 100 μm (**c**, **g**, **h**). (**i**) Model for the biological role of CHD8. When cells proliferate extensively during early embryogenesis, CHD8 is expressed at high levels and suppresses p53 function through histone H1 recruitment to prevent unwanted apoptosis. Once the level of CHD8 expression decreases, during mid to late embryogenesis, some cells undergo apoptosis for organogenesis.

than in newborns. Genetic ablation of CHD8 results in extensive p53-dependent apoptosis in mouse embryos at a stage when *Chd8* is expressed at high levels in wild-type mice. On the other hand, apoptosis is necessary for organogenesis, which occurs mainly during mid to late embryogenesis, when the level of *Chd8* expression decreases. CHD8 may therefore regulate a threshold for apoptosis induction in a developmental-stage-specific manner: The threshold for apoptosis triggered by p53 is high during early embryogenesis, whereas it is lower after the mid-stage. In cancer cell lines, the level of CHD8 is relatively high, suggesting that cancer cells generally show an undifferentiated phenotype and reflect embryonic stages of development, or that cells expressing CHD8 may have a selective advantage in terms of cell growth or acquisition of immortality as a result of the suppressing p53 function. Thus we suggest that p53 function is, at least in part, suppressed by CHD8 in such cancer cell lines. Furthermore, haploinsufficiency at the *CHD8* locus was recently implicated in the pathogenesis of a human developmental anomaly[40], providing further genetic evidence in support of a crucial role for CHD8 in development.

METHODS

Antibodies. Anti-p53 (FL393, Pab240), anti-Mdm2 (SMP14) and anti-His_6 (H15) antibodies were obtained from Santa Cruz Biotechnology; anti-caspase-3 cleaved at Asp-175 and anti-PARP antibodies were from Cell Signalling; anti-histone H1 antibodies were from Abcam; anti-p21 antibodies from BD Pharmingen; anti-Hsp70 and anti-Hsp90 antibodies from Transduction Laboratories; anti-HA (HA11) antibodies from Babco; anti-Myc (9E10) antibodies from Roche; anti-Flag (M2) from Sigma; anti-α-tubulin (TU01) antibodies from Zymed; anti- glyceraldehyde-3-phosphate dehydrogenase (GAPDH; 1D4) from Stressgen; and anti-CHD8 antibodies were generated by A. Kikuchi (Hiroshima University). Alexa 488- or